Flammability, Ignition Energy and Flame Speeds in NH_3-H_2-CH_4-N_2O-O_2-N_2 Mixtures

Ulrich Pfahl and Joseph E. Shepherd

Graduate Aeronautical Laboratories
California Institute of Technology
Pasadena, CA 91125

Explosion Dynamics Laboratory Report FM97-4R1

July 15, 1997

Abstract

This report describes studies on flammability and flame propagation in mixtures of interest to the Flammable Gas Safety Issue for the waste tank farms at the Hanford site. Flammability limits, pressure histories, ignition energy, and flame speeds have been measured for selected mixtures of hydrogen–nitrous oxide–air, methane–nitrous oxide–air, ammonia–nitrous oxide and hydrogen–nitrous oxide–ammonia–nitrogen–methane–air mixtures at initial pressures of 100 kPa. These investigations were accompanied by reactant and product gas-analysis using gas chromatography and Fourier transform infrared spectrometry.

Contents

Executive Summary

This report summarizes flammability and flame propagation studies in FY97 on flammable gases retained in the waste within the tank farm at the Hanford site. This work is a continuation of previous studies at Caltech on the flammable gas issue.

Experiments have been carried out in an 11.25-liter combustion vessel for a wide range of mixtures. Measurements include peak pressure, flammability limits, ignition energy, flame speed, nitrous oxide consumption and product composition. The mixtures studied were hydrogen–nitrous oxide–air, methane–nitrous oxide–air (10% N_2O), ammonia–nitrous oxide and hydrogen–nitrous oxide–ammonia–nitrogen–methane–air mixtures representative of retained gases.

Lower and upper flammability limits and ignition energy bounds of methane–nitrous oxide–nitrogen and ammonia–nitrous oxide–nitrogen mixtures with air have been determined. We investigated the influence of small amounts of oxygen (3 to 5%) on flammability of methane–nitrous oxide–nitrogen mixtures.

The behavior of nitrous oxide consumption in hydrogen–nitrous oxide–air is very different than in methane–nitrous oxide–air or ammonia–nitrous oxide mixtures. Whereas the nitrous oxide completely dissociates during combustion of all flammable methane–nitrous oxide–air and lean ammonia–nitrous oxide mixtures (even with 54% nitrogen dilution) it only partially dissociates for lean hydrogen–nitrous oxide–air mixtures (less than 14% H_2). For barely flammable hydrogen–nitrous oxide–air mixtures (6% H_2), almost no nitrous oxide is consumed. There is a distinct increase in the nitrous oxide consumption as the initial hydrogen concentration is increased from 8% to 9%.

The lower flammability limit of methane–nitrous oxide mixtures occurs at 2.7% methane for ignition energies less than 10 J. This value increases to 4.7% for ignition energies less than 0.04 J. The upper flammability limit is between 40 and 50% methane for ignition energies less than 10 J. Addition of 70% nitrogen will inert the mixture. Small amounts of oxygen (3 to 5%) do not significantly influence the limits or inerting concentration.

The flammability limits of ammonia–nitrous oxide mixtures occur at 5.2% (LFL) and 67.5% (UFL) ammonia for ignition energies less than 10 J. Ignition energy bounds for ammonia–nitrous oxide mixtures were measured for ignition energies between 0.04 J and 8 J at 0 and 54% nitrogen dilution. Addition of 60% nitrogen or 84% air will inert the mixture. A stochiometric ammonia–air (28% ammonia, 72% air) mixture at 100 kPa initial pressure is flammable for ignition energies above 0.7 J.

For ignition energies less than 10 J, the flammability limits of mixture 27 (40% H_2, 40% N_2O, 20% CH_4), mixture 28 (35% H_2, 35% N_2O, 10% CH_4, 20% NH_3) and mixture 29 (29% H_2, 24% N_2O, 11% NH_3, 35% N_2, 1% CH_4) occur at 7%, 9% and 14%. Whereas mixtures 27 and 28 are flammable up to 100% (no air), the upper flammability limit for mixture 29 with air occurs between 90 and 100%. All three mixtures show no pronounced dependence of the lean flammability limit on the ignition energy between 0.04 and 8 J. Flame speeds of mixtures 27 and 28 with air are almost equal between 80 and 90% air (quiescent conditions), whereas the flame speed of mixture 29 with air is much slower.

1 Introduction

The goals of this study are to characterize the combustion behavior of gas mixtures that are relevant to retained gas within the waste in the tank farm located at the Hanford site. The range of compositions present in the retained gas within the waste is illustrated in Table 1, which gives data from recent retained gas sampling activities. The typical average tank temperatures are 40 to 50°C except for A-101, which is 66°C. The thermodynamic characteristics of these fuel-oxidizer combinations is summarized in Tables 2 and 3.

Table 1: Representative retained gas compositions from the waste tanks at the Hanford Site.

Tank	V_{GRE} (m$_3$)	H$_2$ (%)	N$_2$O (%)	N$_2$ (%)	NH$_3$ (%)	CH$_4$ (%)	H$_2$O (%)
Double Shell Tanks							
SY-101	131	29	24	33	11	1	2
AW-101	14	31	4.3	60	.02	1.6	
AN-105	26	63	11	25	.02	0.7	
AN-104	23	47	19	32	.02	0.9	
AN-103	14	61	3.8	34	.05	0.01	
Single Shell Tank							
A-101	-	75	5.6	16	2.4	.7	

Table 2: Standard heats of formation for the species of interest in retained gases.

species	$\Delta_f H°$ (kJ/mol)
NH$_3$	-45.9
CH$_4$	-74.8
N$_2$O	+82.1
CO$_2$	-393.7
H$_2$O	-241.9
H$_2$	0.0
N$_2$	0.0
O$_2$	0.0

Table 3: Standard heats of reaction for fuel-oxidizer combinations found in retained gases.

Reaction	$\Delta_R H°$ (kJ/mol)	ΔN
N$_2$O $\longrightarrow$ N$_2$ + 1/2O$_2$	-82.1	1/2
NH$_3$ + 3/4O$_2$ $\longrightarrow$ N$_2$ + 3/2H$_2$O	-195	3/4
CH$_4$ + 2O$_2$ $\longrightarrow$ CO$_2$ + 2H$_2$O	-857.	0
H$_2$+ 1/2O$_2$ $\longrightarrow$ H$_2$O	-241	-1/2

Flammability of the individual fuels in air is fairly well characterized. Available data on limits is summarized in Table 4. However, there are some peculiar aspects to these fuel-oxidizer combinations, particularly with mixtures containing N$_2$O. N$_2$O decomposes slowly at low temperatures but is extremely exothermic. N$_2$O can behave as an explosive if the ignition stimulus is large enough and there are sufficient H atoms present to catalyze the decomposition. However, for very low temperature flames, the N$_2$O does not appear to react at all. Mixtures of NH$_3$ and air burn very slowly and in many situations are considered to

be nonflammable. However, mixtures of NH_3 and N_2O appear to react much more rapidly. The reaction mechanism of N_2O and NH_3 is particularly uncertain. H_2 has a very large flammablility range and unusually high flame speed.

Table 4: Flammability limits for fuel-air mixtures at NTP. Amounts are given in volume %. LFL = Lower Flammability Limit, UFL = Upper Flammability Limit, DPL = Downward Propagation Limit, UPL = Upward Propagation Limit

| Fuel | LFL | | ST | UFL | Inert (N_2) |
	UPL	DPL			
H_2	4	8	29.6	75	70
CH_4		5	9.5	15	37
NH_3	15	18	22	28	15

Flammability of fuels in N_2O is not as well characterized as in air. At the time we started this study, no information was available on CH_4 limits and the data available for NH_3 was quite limited. Our present data on the limits is given in Table 5.

Table 5: Flammability limits for fuel-N_2O mixtures at NTP. Amounts are given in volume %.

| Fuel | LFL | | UFL | Inert (N_2) |
	UPL	DPL		
H_2	3	6	84	~60
CH_4		5	50	70
NH_3	2.6	6.8	71	60

Understanding of flammability in binary and ternary fuel mixtures (H_2-NH_3-CH_4) is rudimentary. The most common assumption is that the limiting mole fractions X_i of each fuel species i obey Le Chatelier's Rule:

$$\sum_{fuels} \frac{X_i}{X_{i,LFL}} = 1 \quad \text{at mixture LFL} \tag{1}$$

where $X_{i,LFL}$ is the limit concentration for a single fuel species i in the oxidizer-diluent mixture of interest. The effect of multiple oxidizers (O_2, N_2O) on flammability limits is not well understood.

Our present understanding of the pressure loads in these mixtures is based on simple but reliable ideas. A standard approach is to use constant volume explosion estimates (AICC- adiabatic, isochoric, complete combustion) based on chemical equilibrium ideas. For this purpose, we use the computer program STAN-JAN which is based on the JANNAF thermochemistry data and minimization of Gibbs energy. Although reasonably reliable, there are some cautions about using these values in safety assessments:

1. Incomplete combustion occurs near the LFL for H_2 and NH_3

2. There are cellular instabilities and a strong Lewis number effect for H_2

3. N_2O undergoes partial or no reaction in lean mixtures

4. Ignition energies are very high for large amounts of N_2O and small amounts of fuel

In general, it is found that H_2 dominates behavior of mixtures. Estimates of peak pressure and temperature in fuel-air explosions are given in Fig. 1, and for fuel-N_2O mixtures in Fig. 2.
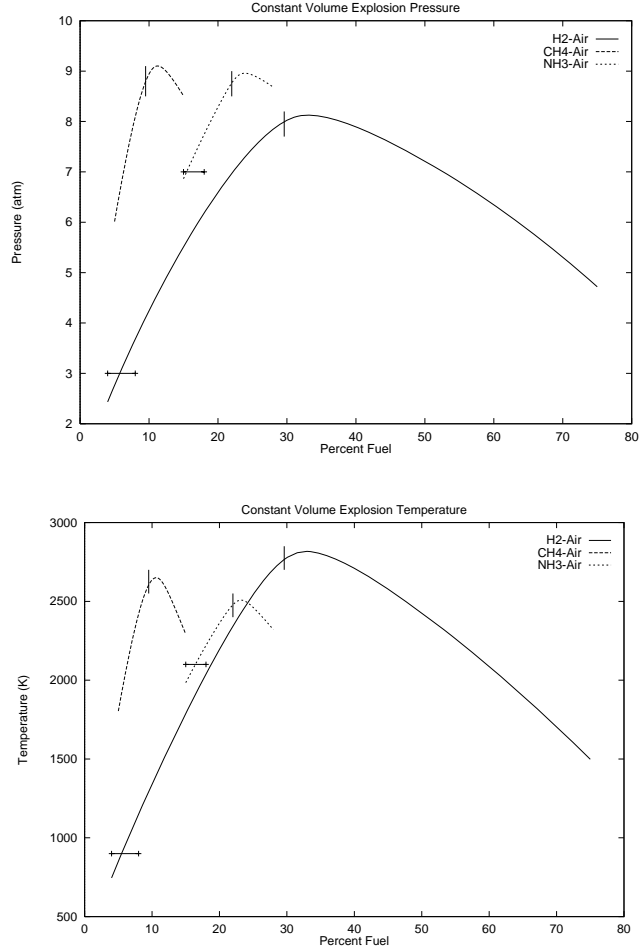
Figure 1: Constant volume explosion pressures and temperatures in fuel-air mixtures, initial conditions of 1 atm and 295 K.

1.1 The Present Study

One focus of the present study is to develop information on fuel-N_2O systems over a wide range of dilution. The previous work (Ross and Shepherd 1996) considered primarily the lean flammability behavior of the following mixtures:

1. H_2-N_2O-Air

2. NH_3-N_2O-Air

3. H_2-NH_3-Air

4. Four-Part Mixtures (A - D given in Table 6)

In the present study we have concentrated on measuring flammability maps, ignition energy bounds, and product compositions. We consider these same fuels but focus on N_2O as the oxidizer with N_2 and air dilution. We have also re-examined the selected blends (A - D) of Table 6, and considered four new blends labeled mixtures 27 -29. The numbers in parentheses refer to the original notation of Ross (1996).

The plan of this document is to first present the details of the facility, concentrating on the differences from the previous setup. Then the gas sampling system and calibrations will be described. Following this background, we discuss results for each of the gas compositions we have studied.

3
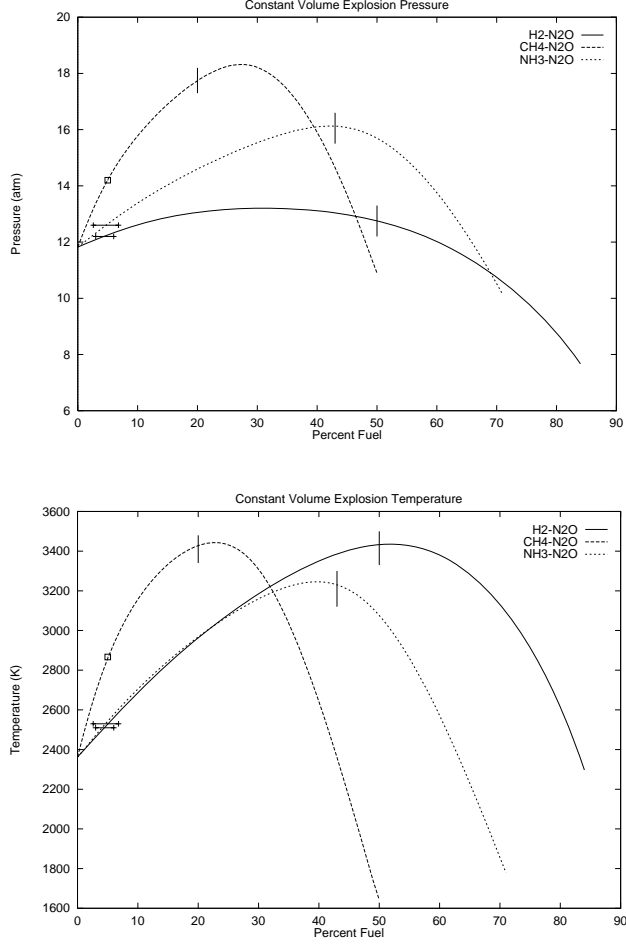
Figure 2: Constant volume explosion pressures and temperatures in fuel-N_2O mixtures, initial conditions of 1 atm and 295 K.

Table 6: Fuel blends A-D (also considered in original study) and blends 27-29 considered in the present study.

Mixture	H_2 (vol %)	N_2O (vol %)	NH_3 (vol %)	CH_4 (vol %)	N_2 (vol %)
A (26)	42	36	21	1	0
B (11)	35	35	30	0	0
C (12)	25	25	50	0	0
D (20)	16.7	33.3	50	0	0
27	40	40	0	20	0
28	35	35	20	10	0
29	29	24	11	1	35

4

2 Facility

The present experiments were done in a combustion vessel Mini-CONVOL (MCV in Fig. 3) which has a volume of 11.25 liters. The vessel is constructed of steel slabs and forms a rectangular chamber with internal dimensions of 190 mm × 203 mm × 305 mm.

The gas-supply and vacuum system, instrumentation, and data acquisition are identical to those used in the previous study (Ross and Shepherd 1996). The vessel can be evacuated, filled with a mixture of gases using partial pressures to determine composition and the products are exhausted through a treatment system following combustion. Special precautions, described in Ross and Shepherd (1996), are taken when using ammonia. To make gas analysis possible we connected the vessel, gas chromatograph, and fourier transform infrared spectrometer by a sampling loop (see GC and FTIR in Fig. 3). This loop can be evacuated and the test gas is pumped through the system to get a homogeneous mixture.

All investigations were carried out under turbulent gas conditions except tests to measure flame speeds under quiescent conditions for mixtures 27 - 29. The turbulence was produced by a single mixing fan with two blades, about 150 mm in diameter. The mixing fan is driven by a pulley drive (6.7:1 reduction) from a universal motor controlled by a speed control (light-dimmer switch). The shaft for the fan was connected to a magnetic torque transmitter which is located at the top of the vessel. Flow measurements were made[1] near
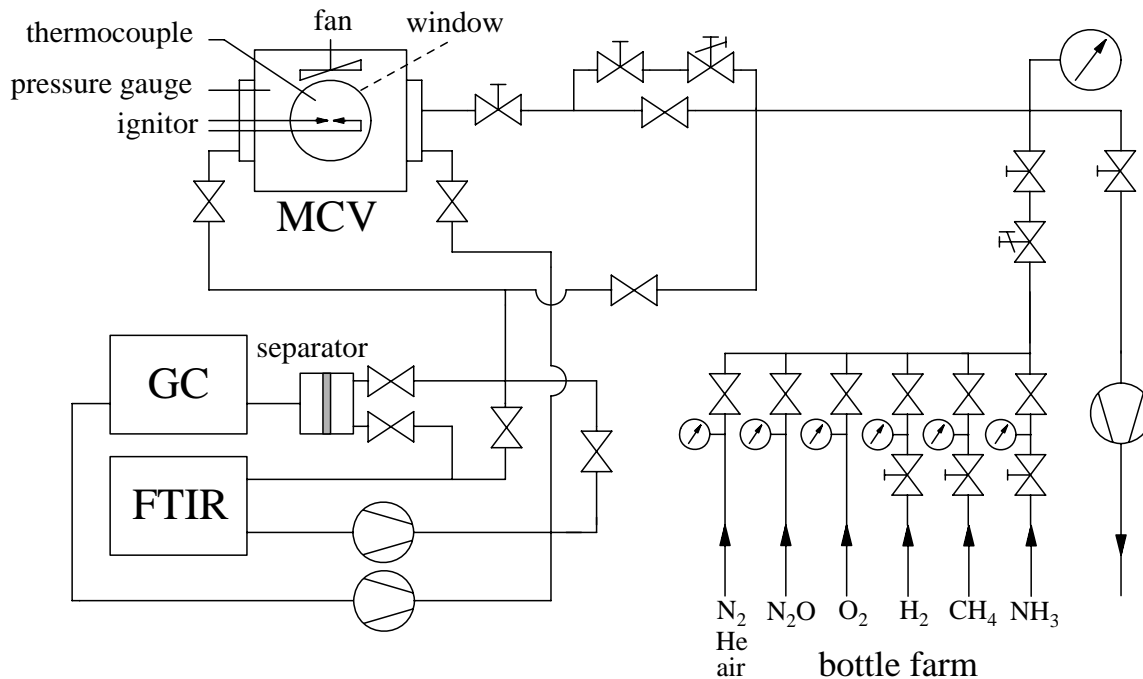

Figure 3: Schematic diagram of the constant volume vessel, gas supply, vacuum system and the gas sampling facilities.

the ignition location with a single-component laser doppler anemometer (LDA). The signals were processed with a Dantec model 55L96 counter to obtain mean $\overline{u}$ and fluctuating velocities u_{rms} in the vertical direction. The result of these measurements is given in Table 7. Mean flow and fluctuations increase with fan rotational speed, however the turbulence intensity $u' = u_{rms}/\overline{u}$ is found to be relatively independent of the rotational speed. Measurements at various locations also indicate that the turbulence intensity is relatively independent of position. The combustion vessel is instrumented with a pressure gauge and a thermocouple (see Fig. 3). After passing through signal conditioning units, the output of these gauges is recorded on a digital data

---

[1]The authors thank Kumar Raman for carrying out these measurements.

Table 7: Mean flow and turbulent intensity near the ignition location.

Fan speed	$\overline{u}$ (m/s)	u_{rms} (m/s)	u'
low	0.41	0.10	0.24
medium	0.65	0.17	0.26
high	0.85	0.22	0.26

acquisition system.

The vessel is equipped with 25-mm thick glass windows with a clear aperature of 117-mm diameter. Through these windows, a color-schlieren video-system is used to observe the flame initiation and propagation. Figure 4 shows a schematic diagram of the optical set-up of the color-schlieren video-system.
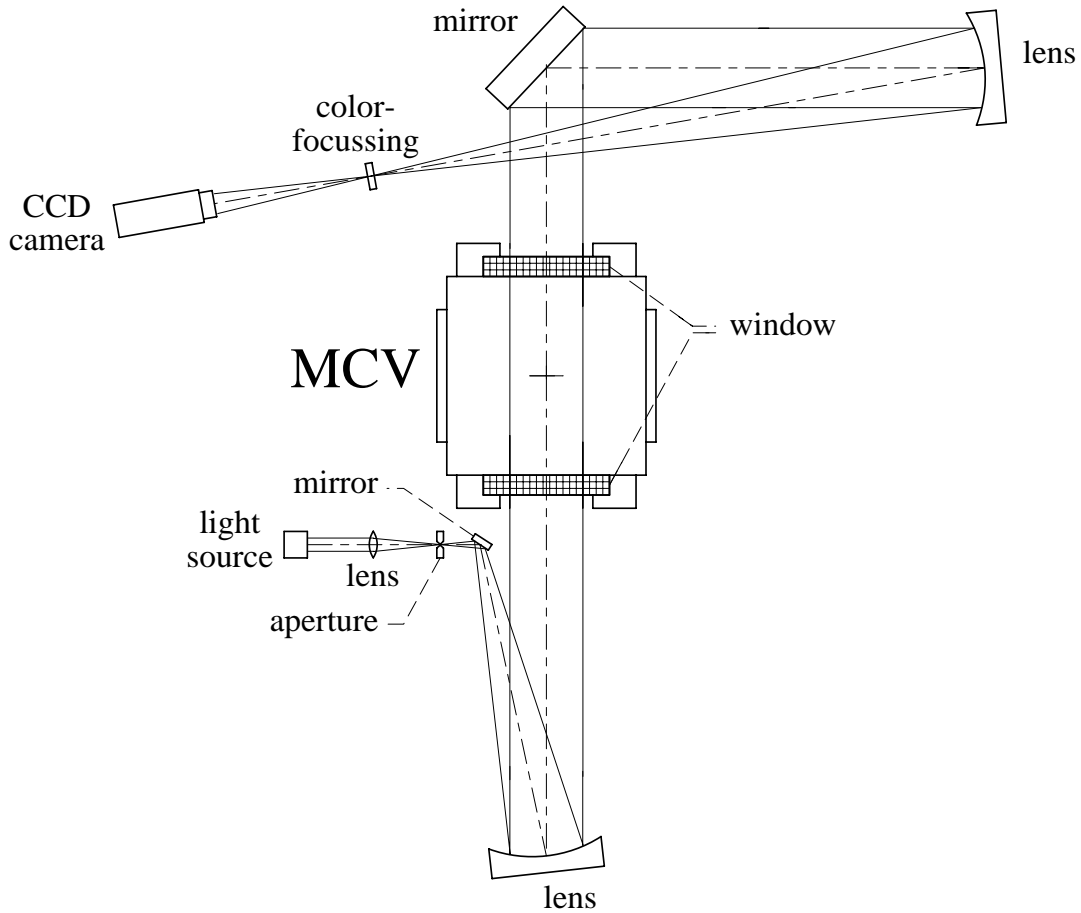
Figure 4: Schematic diagram of the color-schlieren video-system.

An electric spark is used to initiate the flame. The spark gap (2-5 mm depending on the composition) is positioned in the center of the vessel and the electrodes pass through Teflon insulators on the sides of the vessel. The power for the spark is provided by a 0.5 μF capacitor charged by a Hipotronics 15 kV power supply. The discharge across the gap is triggered by a 30 kV pulse (low current) from an EG&G TM-11A power supply. Figure 5 shows a schematic diagram of the most recent circuit of the spark ignition system.

The circuit is motivated by the design described in Ronney (1985).

Figure 5: Schematic diagram of the spark ignition system.

3 Reactant and Product Gas Analysis

The experimental studies reported subsequently were mostly carried out using pre- and post-burn gas analysis. For these analyses, the Gas Chromatograph (GC) and the Fourier Transform Infrared Spectrom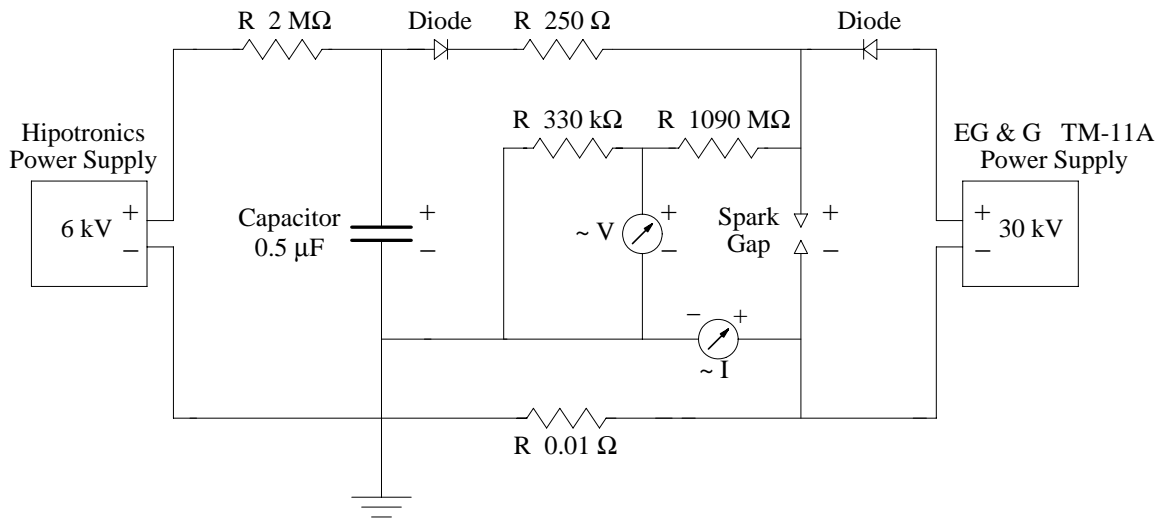eter (FTIR) were used. The measured substances are the fuels H_2 and CH_4, the oxidizers N_2O and O_2, and also the inert component N_2.

3.1 Gas Chromatography

In the present investigations, the MTI Analytical Instruments *M200 Micro Gas Chromatograph* with two columns (column A: molecular sieve MS-5A 10m, column B: poraplot Q OV-1 4m, 2μm) was used. The instrument was supplied from Westinghouse Hanford Company and set up by H.A. Frey and C.J. Hewitt of CST-6, Los Alamos.

Figures 6 and 7 show examples of one pre- and one post-burn chromatogram of run 246. The pre-burn partial pressures were: 8.6 kPa H_2, 10.0 kPa N_2O (GC: 9.8 kPa, FTIR: 10.2 kPa), 17.3 kPa O_2 and 62.8 kPa N_2. The post-burn partial pressures were: 0.3 kPa H_2, 6.0 kPa N_2O (GC: 5.7 kPa, FTIR: 6.3 kPa), 14.1 kPa O_2 and 78.7 kPa N_2.


```
Channel: A
Current Time: Apr 02, 1997  17:15:22
Method: c:\uli\gc\method\01_24_97.met
File  : c:\uli\gc\data\g246i.2
Data file creation time: Feb 10, 1997  10:57:30
Instrument ID: •
Column Type: 1xOct 21, 1996  15:30:48
Carrier Gas:
Column Head Pressure: 30.1 psi
Column Temperature: 45 C
Instrument Gain: LOW
Sample Time:   5 seconds
Inject Time: 30 milliseconds
Run Time: 100 seconds
```

```
Channel: B
Current Time: Apr 02, 1997  17:15:44
Method: c:\uli\gc\method\01_24_97.met
File  : c:\uli\gc\data\g246i.2
Data file creation time: Feb 10, 1997  10:57:30
Instrument ID: •
Column Type:  15:30:48
Carrier Gas:
Column Head Pressure: 27.6 psi
Column Temperature: 50 C
Instrument Gain: LOW
Sample Time:   5 seconds
Inject Time: 40 milliseconds
Run Time: 100 seconds
```
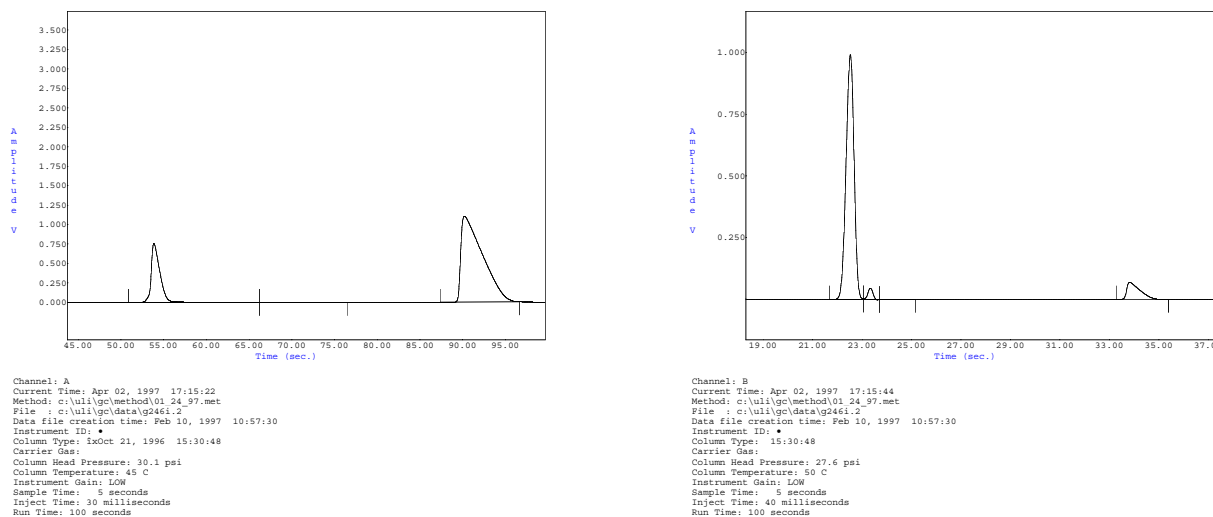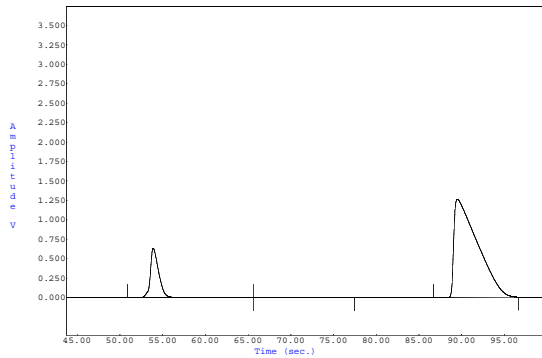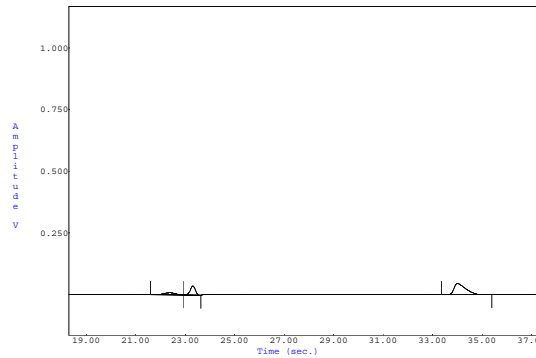
Figure 6: GC results for run 246, pre-burn; channel A: 1st peak (RT = 54.1 s) 17.3 kPa O_2, 2nd peak (RT = 90.9 s) 62.8 kPa N_2; channel B: 1st peak (RT = 22.5 s) 8.6 kPa H_2, 3rd peak (RT = 34.0 s) 9.8 kPa N_2O.

Both calibrations between measured area counts and the gas partial pressure, and also all gas analysis were done at a total pressure of 100 kPa. In case the post-burn total pressure differs more than $\pm$ 2 kPa from 100 kPa (which is usually the case), the pressure was corrected by filling with nitrogen or by evacuation. The composition results were then corrected to compensate for this change in pressure in the vessel. This was found to be an important step in carrying out accurate measurements with the GC. Another important step in the procedure was to bake the molecular sieve column out at 180°C overnight under a vacuum before each set of measurements. Even though the inlet to the GC used a H_2O membrane separator (A+ corporation,

Figure 7: GC results for run 246, post-burn; channel A: 1st peak (RT = 54.1 s) 14.1 kPa O_2, 2nd peak (RT = 90.3 s) 78.7 kPa N_2; channel B: 1st peak (RT = 22.4 s) 0.3 kPa H_2, 3rd peak (RT = 34.1 s) 5.7 kPa N_2O.

genie model 101), such large quantities of H_2O are produced in this experiment that the daily bake out is needed to remove H_2O from the molecular sieve column. Otherwise large shifts in the retention times and concentration-area relationships were observed. GC sampling times were also reduced to a minimum and the detectors operated at the lowest sensitivity to avoid saturation. The sample loop also had to be operated in a very consistent fashion in order to get consistent results. By carrying out all of these steps, excellent repeatability was obtained with the GC. As shown in Figs. 8 - 12, the resulting area-concentration relationship are very linear and repeatable over calibrations taken weeks apart.

The molecular sieve (column A) was used to quantify oxygen (0 - 20 kPa) and nitrogen (0 - 95 kPa). The retention times are about 54 s for oxygen and 87 s for nitrogen. Figures 8 and 9 show the calibration between the area counts and the gas partial pressure.

The poraplot Q (column B) was used to quantify hydrogen (0 - 24 kPa), methane (0 - 24 kPa) and nitrous oxide (0 - 15 kPa). The retention times are about 22.5 s for hydrogen, 25.5 s for methane and 34 s for nitrous oxide. Figures 10 to 12 show the calibration between the area counts and the gas partial pressure for these three components.
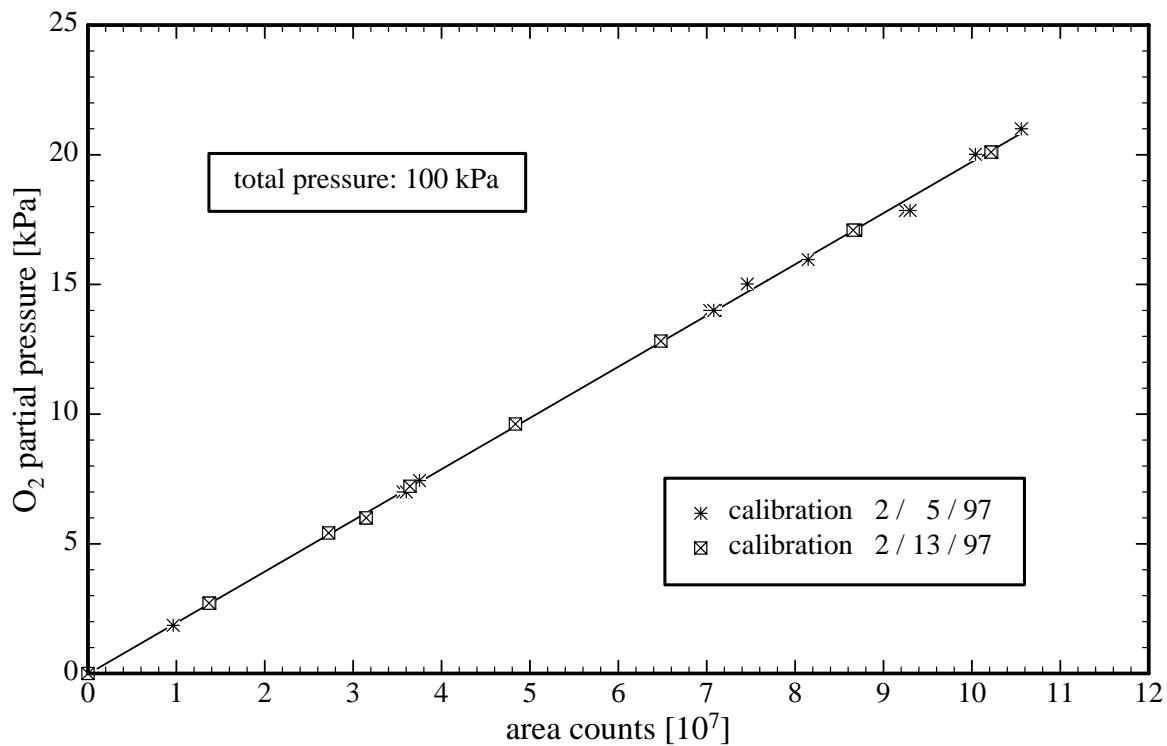
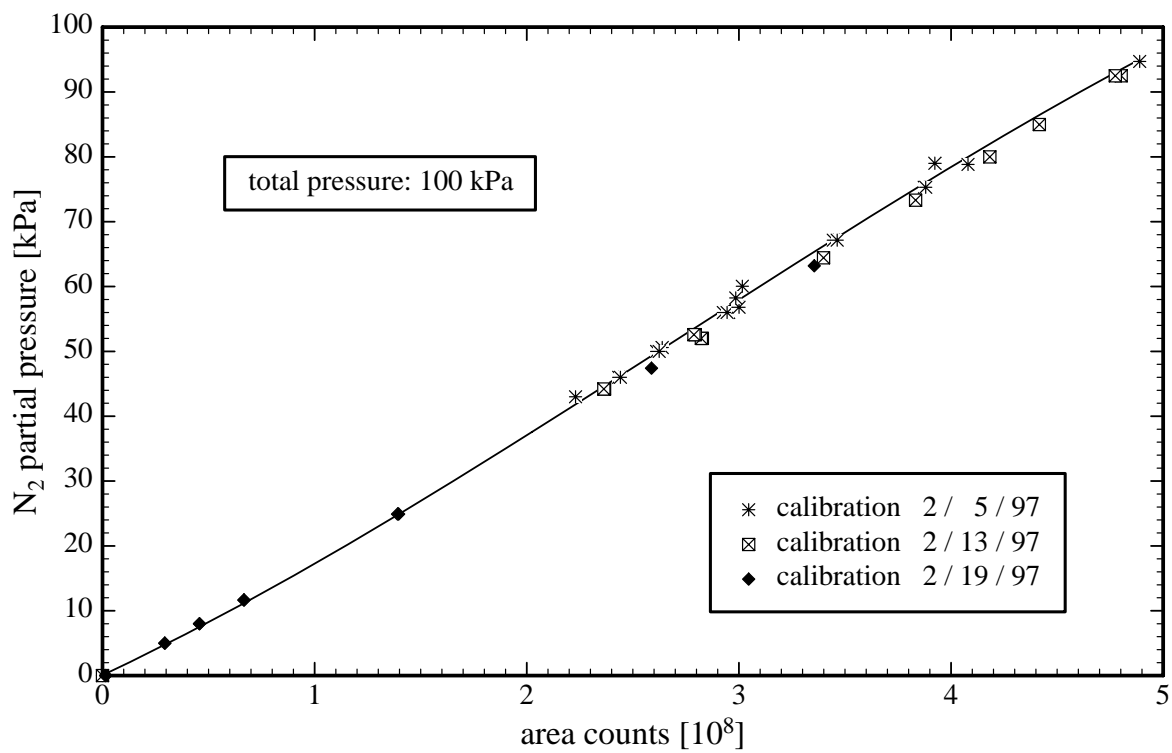Figure 8: Gas chromatograph calibration for oxygen.

Figure 9: Gas chromatograph calibration for nitrogen.
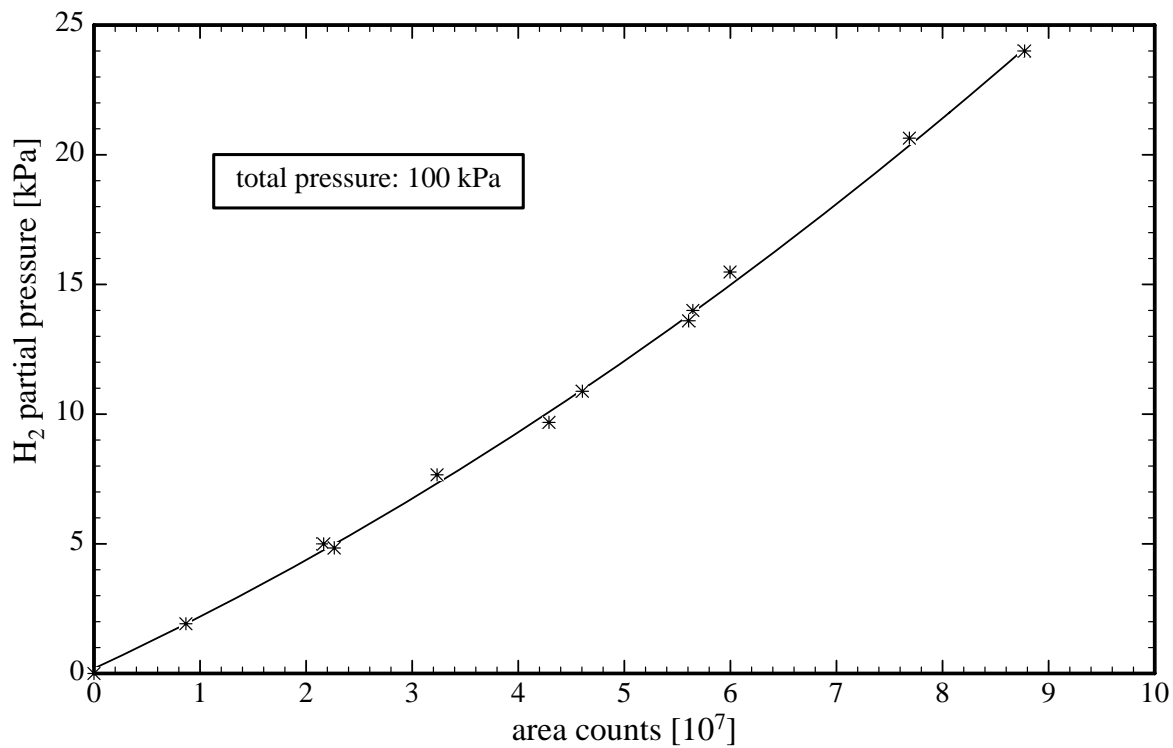
Figure 10: Gas chromatograph calibration for hydrogen.
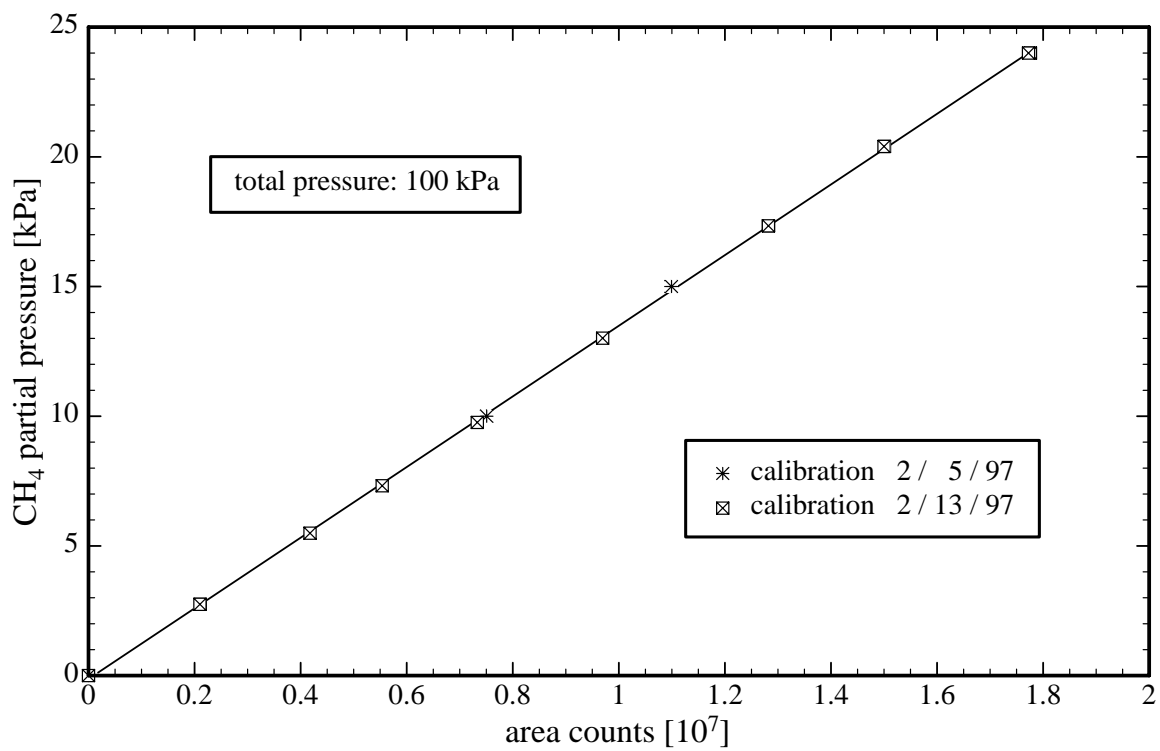
Figure 11: Gas chromatograph calibration for methane.
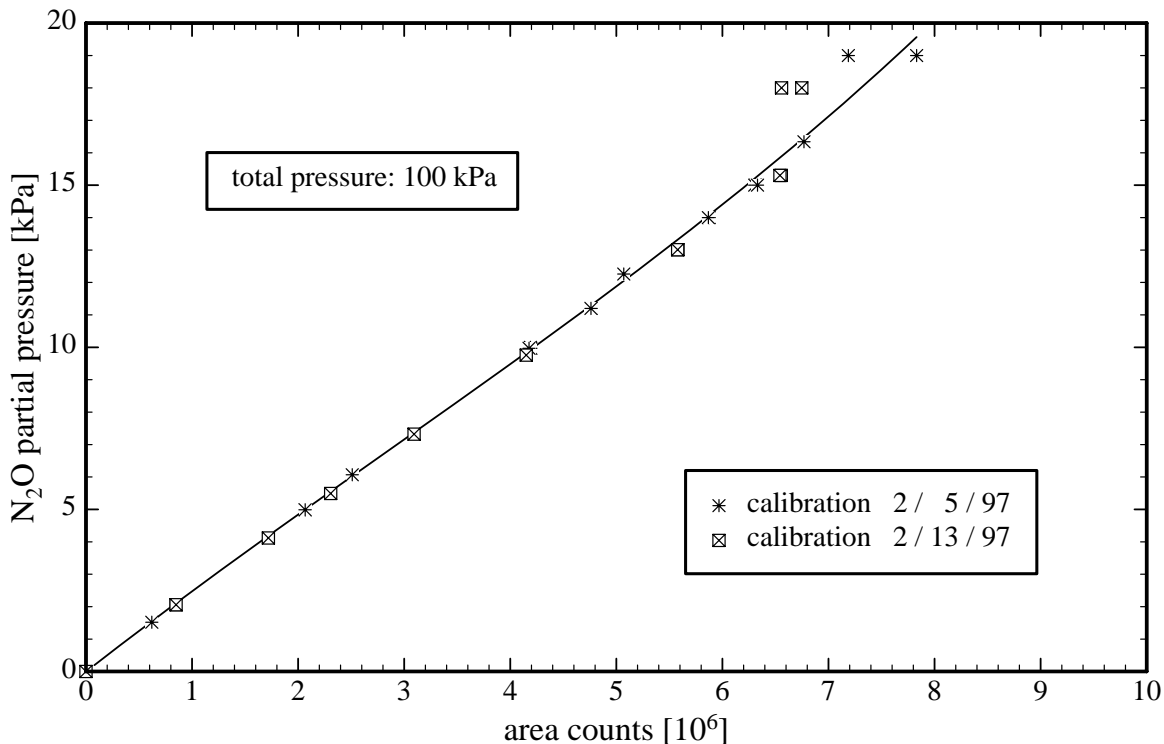
Figure 12: Gas chromatograph calibration for nitrous oxide.

3.2 Fourier Transform Infrared Spectrometry

The MIDAC Corporation *M2000 FTIR Spectrometer System* was used to quantify the gas partial pressure of nitrous oxide and methane. The basic theory of operation of this spectrometer system is given by Beer's law. This law states that for parallel, monochromatic radiation that passes through an absorber of constant concentration, the transmittance of a stable solution is an exponential function of the concentration of the absorbing solute:

$$log\left(\frac{1}{T}\right) = A = \alpha \cdot b \cdot C \tag{2}$$

where

T	=	transmittance
A	=	absorbance
α	=	absorptivity or extinction coefficient
b	=	optical path length
C	=	molar concentration of the absorbing species

The FTIR measures the transmittance T as a function of wavelength λ or wavenumber $1/\lambda$. A constant extinction coefficient $\alpha(\lambda)$ gives a linear relationship between concentration and absorbance for each absorbing species at a selected wavelength. However, the extinction coefficient is actually a function of the gas concentration so that a nonlinear relationship exists between concentration and absorbance. This relationship was determined by calibration tests in which the FTIR cell was filled by the method of partial pressures with known amounts of the test gases. The absorbance spectrum $A(\lambda)$ was then analyzed to determine the appropriate range of wavelengths for carrying out the calibration between absorbance and gas concentration (partial pressure). It is important to choose a spectral range that is not obscured by water vapor (always present in the spectrum) or other IR-active gases in the system. A spectral range with a low extinction coefficient is also desirable in order to obtain a large dynamic range. Many of the N_2O bands are so intense that the absorbance saturates at high concentration.

Figure 13 shows the pre-burn raw transmission spectrum of run 246 (left) and the raw transmission spectrum of air at 100 kPa (right) which was used as the background spectrum. The spectral features in the background are due to the wavelength dependence of the source radiosity and the absorbance of water vapor ubiquitously present as a contaminant in the light path. Figure 14 shows the pre- and post-burn reduced absorbance spectra of run 246. These absorbances are obtained from the logarithm of the ratio of the raw transmission signals for the sample to that of the background. The pre- and post-burn partial pressures of nitrous oxide were 10.0 (GC: 9.8 kPa, FTIR: 10.2 kPa) and 6.0 kPa (GC: 5.7 kPa, FTIR: 6.3 kPa). Since the GC and FTIR gave slightly different results for composition, we report compositions in the subsequent discussion and tables based on the average of the FTIR and GC values for CH_4 and N_2O.
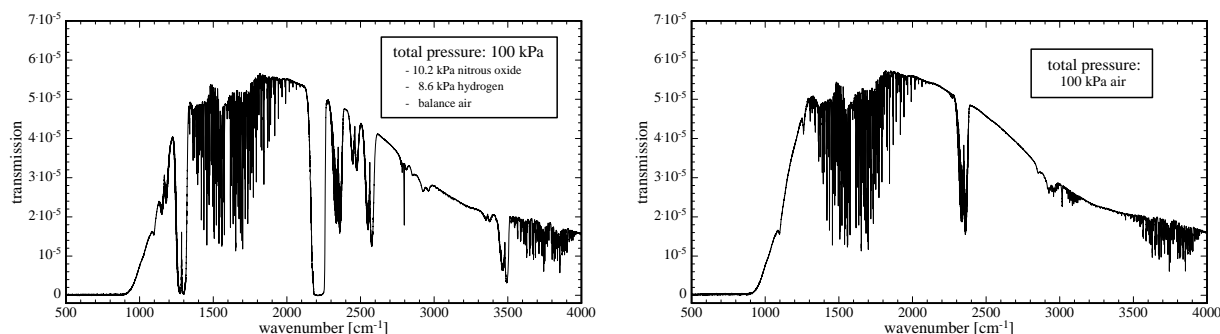
Figure 13: Left: pre-burn raw transmission spectrum run 246; right: background raw transmission spectrum, 100 kPa air.
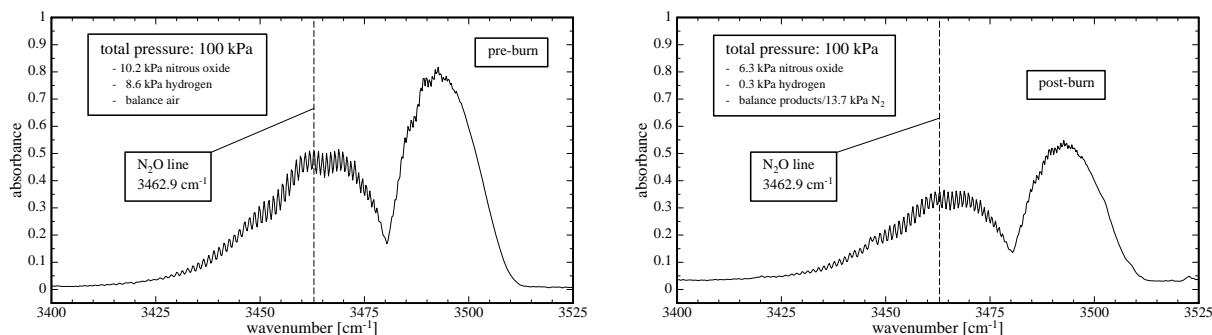
Figure 14: Absorbance corrected for background; left: pre-burn run 246, 10.2 kPa N_2O; right: post-burn run 246, 6.3 kPa N_2O.

For nitrous oxide, a very reliable calibration between gas partial pressure and absorbance could be found from 0 to 15 kPa at the wavenumber 3462.9 cm^{-1} (see Fig. 15), whereas for methane at the wavenumber 3017.7 cm^{-1} no satisfactory calibration could be obtained (see Fig. 16). The reason for this is the choice of the wavenumber (pointed out by H. Frey of CST), the absorbance does not vary much with the methane concentration and the signal-to-noise ratio is too low because the absorbance is too large (> 0.3). A shift of the wavenumber to other values and even an integration of the wavenumber from 3133.5 to 3167.2 cm^{-1} did lead to better but still not very accurate results. Similar problems occurred for ammonia calibrations based on integration from 1663.5 to 1685.9 cm^{-1}. Generally, all FTIR calibrations were very inaccurate for ammonia (irrespective of the wavenumber range) whereas the GC calibrations for oxgen, nitrogen, hydrogen, methane and nitrous oxide were not affected.
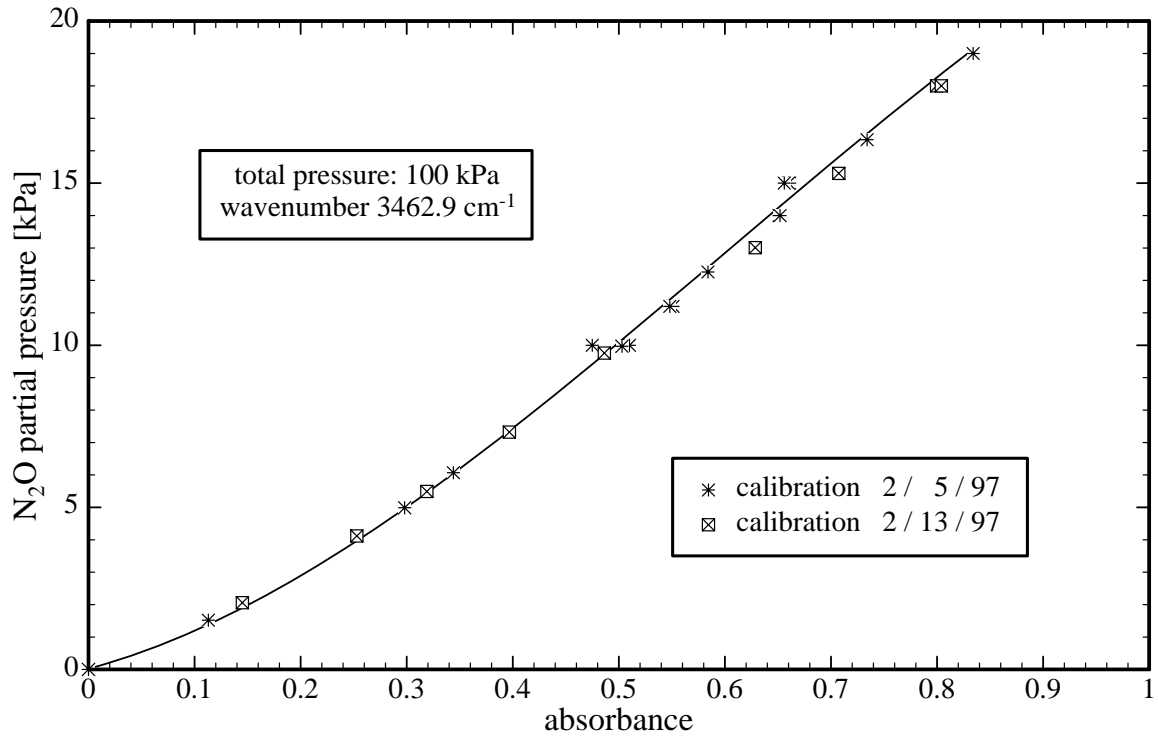
Figure 15: FTIR calibration for nitrous oxide.
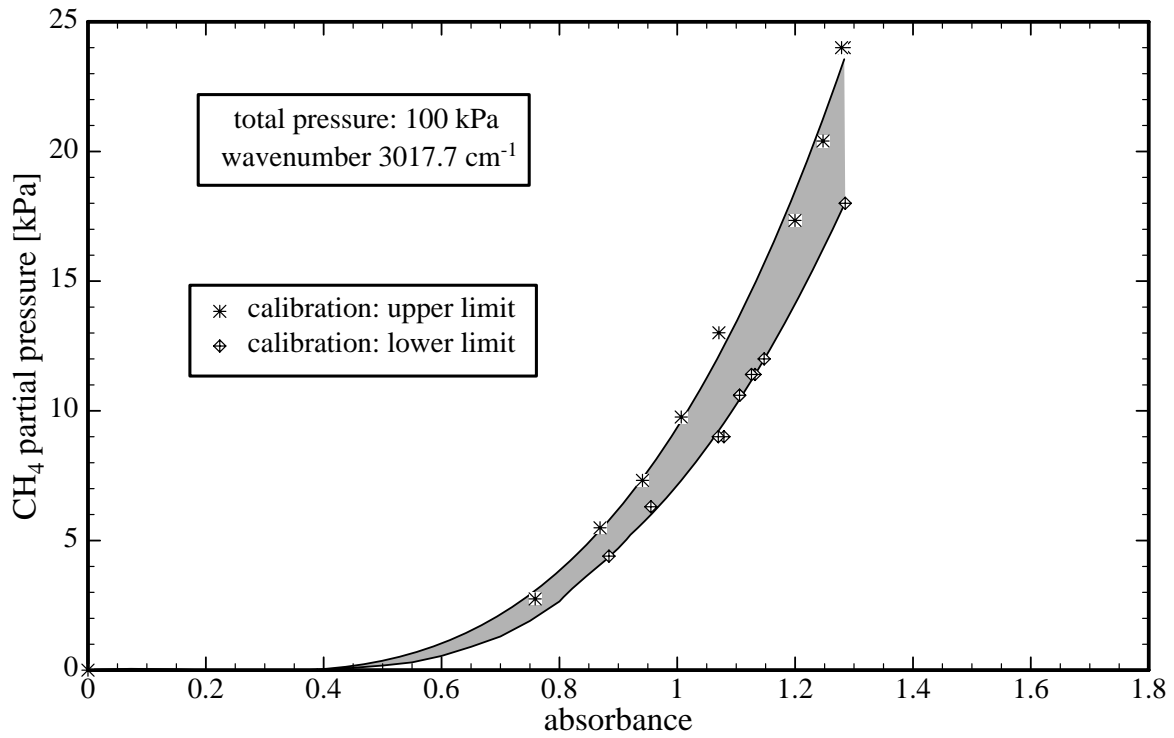
Figure 16: FTIR calibration for methane.

4 Nitrous Oxide Consumption

By analyzing the pre- and post-burn gas composition, (see Section 3) the nitrous oxide consumption during combustion of fuel–nitrous oxide(–air) mixtures was measured. The mixtures investigated were hydrogen–nitrous oxide–air, methane–nitrous oxide–air, ammonia–nitrous oxide and mixtures A–D with air. For all tests, the pre-burn total pressure was 100 kPa and for the hydrogen–nitrous oxide–air and methane–nitrous oxide–air tests the gas partial pressure of nitrous oxide was nominally 10 kPa.

4.1 Hydrogen–Nitrous Oxide–Air Mixtures

For these investigations, the initial gas partial pressure of hydrogen was varied from 5.7 to 13.9 kPa, whereas the initial partial pressure of nitrous oxide was nominally 10 kPa. Figure 18 shows five typical pressure histories for these tests. The peak pressure increases with increasing H_2 concentration: 2.4 bar (5.7 kPa H_2), 3.3 bar (7.5 kPa H_2), 4.0 bar (8.6 kPa H_2), 5.1 bar (10.2 kPa H_2), 6.5 bar (13.9 kPa H_2).

These results are very similar to what was obtained in the earlier study (Fig. 17) in the larger vessel, CONVOL (400 l capacity) (Ross and Shepherd 1996) and the Bureau of Mines 120-l vessel (Cashdollar et al. 1992). There are some differences since the N_2O concentration is held fixed in the present experiments and was variable (proportional to the H_2 concentration) in the Bureau of Mines experiments. However, the values for turbulent conditions appear to define a clear upper bound to the peak pressure that is a continuous function of H_2 concentration down to 4%. The quiescent values show the characteristic sharp cutoff at 8% hydrogen corresponding to the downward propagation limit.
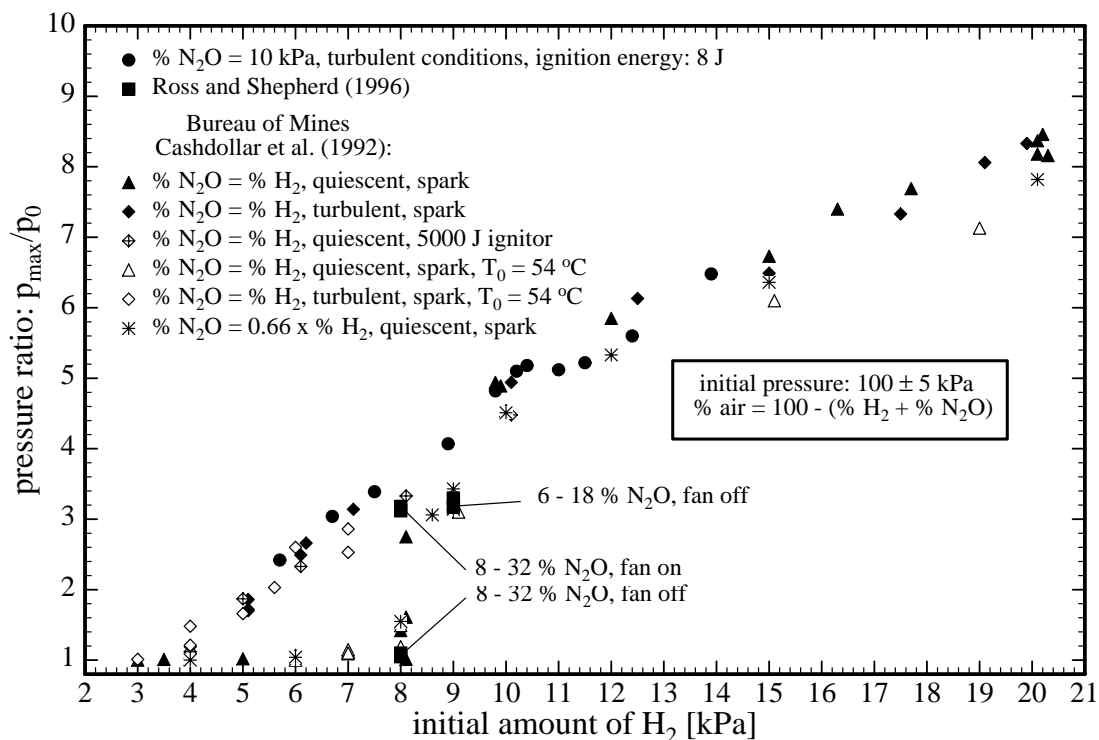
Figure 17: Peak combustion pressure in lean hydrogen–nitrous oxide–air mixture combustion.

The values of initial and final gas partial pressures of H_2 and N_2O, of target and actual final pressures and of peak pressures of the H_2–N_2O–air runs are shown in Table 8. The H_2 final pressure varies between 0.2 and 0.6 kPa for initial H_2 above 6.7 kPa, for run 250 with an initial value of 5.7 kPa H_2 the final amount increases to 1.4 kPa. This indicates complete combustion for all concentrations except at the leanest, 5.7%

Run No.	initial H_2 [kPa]	initial N_2O [kPa]	final N_2O [kPa]	final H_2 [kPa]	target final pressure [kPa]	+ 2.5 kPa H_2O (g) [kPa]	actual final pressure [kPa]	peak pressure bar
250	5.7	10.0	9.15	1.4	92.0	94.5	94.4	2.42
248	6.7	10.2	8.9	0.3	90.5	93.0	91.9	3.04
243	7.5	9.9	8.65	0.6	89.2	91.7	91.0	3.39
246	8.6	10.0	6.0	0.3	89.0	91.5	90.3	-
251	8.9	9.8	4.5	0.3	89.2	91.7	90.2	4.07
244	9.8	9.95	1.75	0.6	89.4	91.9	90.0	4.82
253	10.2	10.15	0.95	0.2	89.2	91.7	89.5	5.10
247	10.4	10.0	0.85	0.3	88.8	91.3	89.4	5.18
252	11.0	10.1	0.65	0.2	88.2	90.7	88.6	5.12
254	11.5	10.2	0.5	0.3	87.5	90.0	87.5	5.22
249	12.4	10.3	0.35	0.3	86.0	88.5	86.6	5.60
242	13.9	10.15	0.15	0.2	83.9	86.4	84.7	6.48

Table 8: Initial and final gas composition, target and actual final pressure and peak pressure of H_2–N_2O–air runs.

H_2.

Figure 19 shows the results of the nitrous oxide consumption during hydrogen–nitrous oxide–air mixture combustion. At 5.7 kPa initial H_2 almost no nitrous oxide is consumed. The final nitrous oxide amounts to 9.15 kPa and the final pressure of hydrogen amounts to 1.4 kPa. With an increasing amount of initial hydrogen the final amount of hydrogen varies between 0.2 and 0.6 kPa, whereas the final amount of nitrous oxide decreases. Above 10 kPa initial hydrogen, the final nitrous oxide amount is below 1 kPa and at 13.9 kPa initial hydrogen the nitrous oxide is almost completely consumed (0.15 kPa).

The results shown in Fig. 19 are the first quantification of the N_2O participation effects. These effects were noted in Cashdollar et al. (1992) but they were unable to make quantitative measurements due to problems with their gas sampling system. Ross and Shepherd (1996) were not equipped to do gas sampling and examined variations in final pressure to attempt to determine the participation limit for H_2-N_2O-NH_3 mixtures. A value of 13% fuel was estimated for the critical amount needed to fully react the N_2O. The present results indicate that a value of 10% is more appropriate when the fuel is H_2, and as discussed subsequently, as little as 5% is required when the fuel is CH_4. As discussed in the next section, the final pressure analysis systematically underestimates the amount of N_2O reacted, resulting in higher participation thresholds.

4.1.1 Final Pressure Evaluation

The measured final pressure in the vessel after the combustion and cooling of the products to room temperature provides additional information about the combustion process. This value (compared to calculations) has been used in previous studies to get some insight into the possible set of product compositions.

Figure 20 shows comparisons between measured (actual) and calculated final pressures (STANJAN or target) for hydrogen–nitrous oxide–air and hydrogen–air mixtures. All values are given in Tables 8 and 9. Calculations were done by using STANJAN (Reynolds 1986). Adiabatic combustion at constant volume is used to define an ideal explosion pressure, temperature and product composition. A constant volume cooling process with condensation of water was then assumed in order to compute the final pressure. The nitrous oxide in the reactants was divided into a reacting and an inert part corresponding to the nitrous oxide consumption measured in the experiments. All gaseous products were taken into account in these calculations. The partial pressure of water was fixed at 2.5 kPa corresponding to the saturation pressure of water at 21°C.
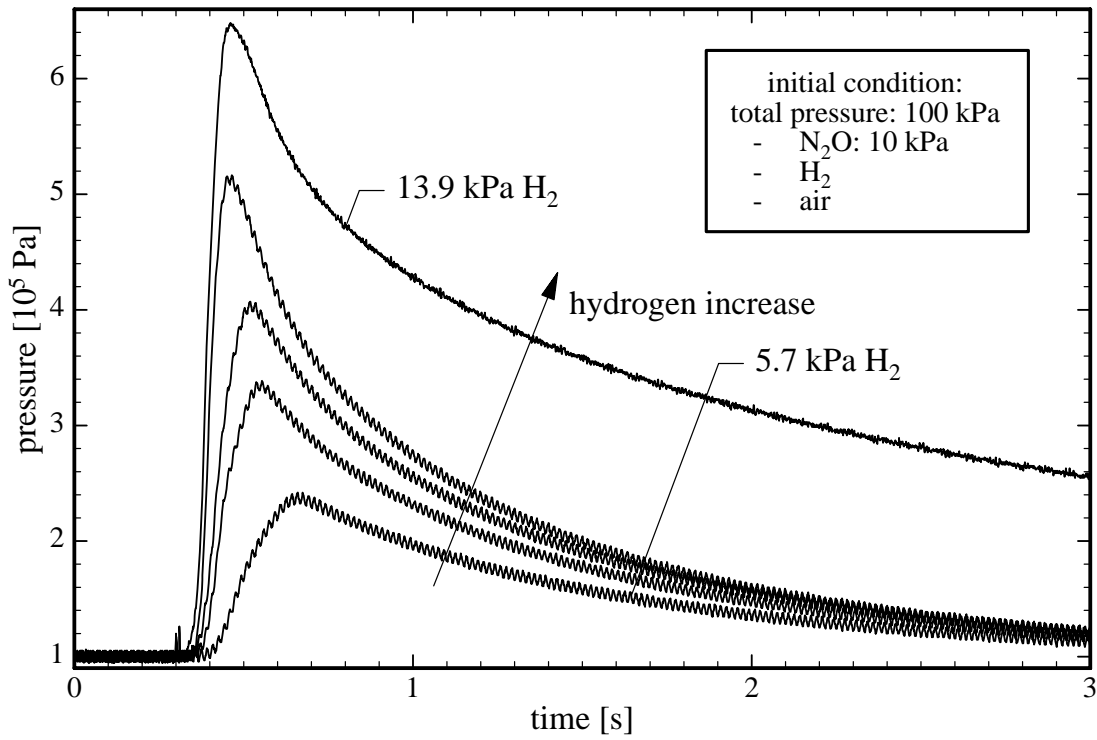
Figure 18: Combustion pressure histories of hydrogen–nitrous oxide–air mixtures.
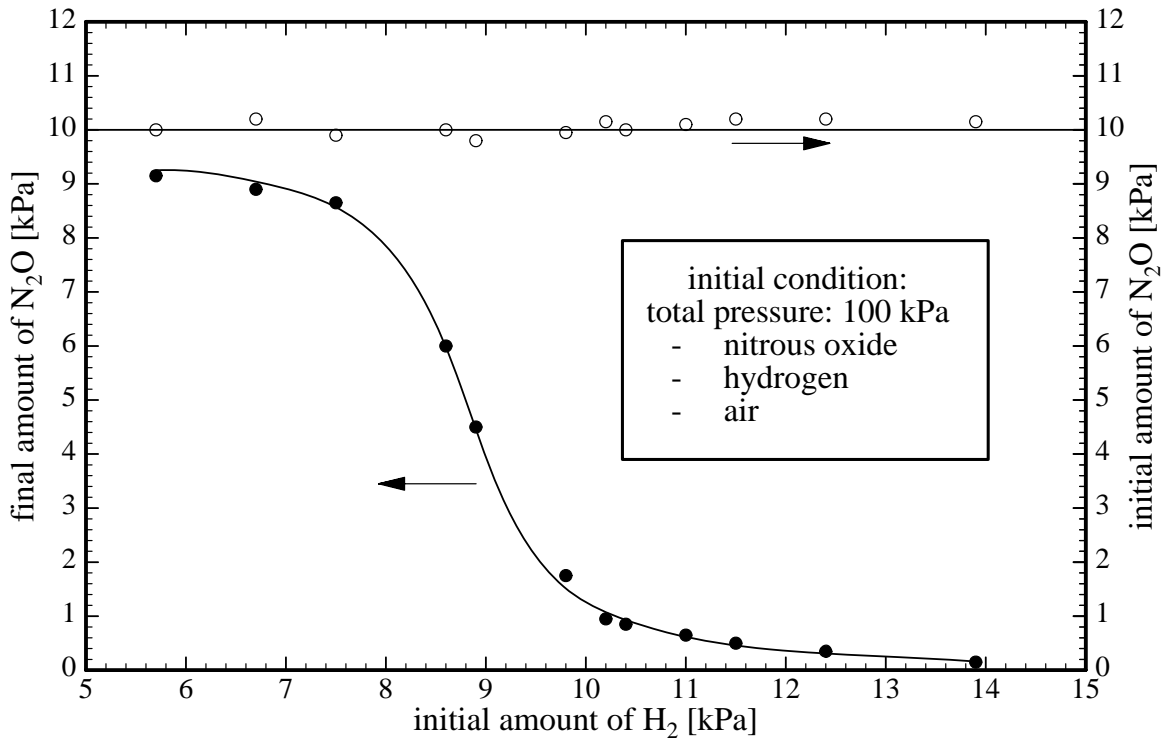
Figure 19: Nitrous oxide consumption in lean hydrogen–nitrous oxide–air combustion.

Run No.	initial H$_2$ [kPa]	initial air [kPa]	final H$_2$ [kPa]	target final pressure [kPa]	+ 2.5 kPa H$_2$O (g) [kPa]	actual final pressure [kPa]	peak pressure bar
280	5.5	94.5	0.0	91.7	94.2	94.8	2.2
282	7.6	92.4	0.0	88.4	90.9	89.6	3.3
278	9.6	90.4	0.1	85.3	87.8	85.8	4.1
281	11.6	88.4	0.0	82.4	84.9	83.7	4.8
279	13.6	86.4	0.1	79.3	81.8	81.0	5.1

Table 9: Initial gas composition, target and actual final pressure and peak pressure of H$_2$–air runs.

The difference between actual and STANJAN values may be caused by either condensed components which are not taken into account by the STANJAN calculations or systematic errors in measurement of temperature and correction for water vapor. A comparison between the two different mixtures (with and without N$_2$O) shows similar differences between actual and target final pressure. This indicates that the putative liquid compounds do not contain significant amounts of nitrogen, making this an unlikely explanation. More probable is that the vessel temperature is nonuniform and not equal to the thermocouple temperature. This creates an uncertainty in the fraction of water condensed which will propagate as a systematic error in the estimated final pressure. Much greater care in the vessel temperature control and more detailed measurements of the gas and wall temperatures would be needed to improve the accuracy of the final pressure technique. The present gas sampling system is an effective solution to the composition measurement issue that avoids this additional complexity.
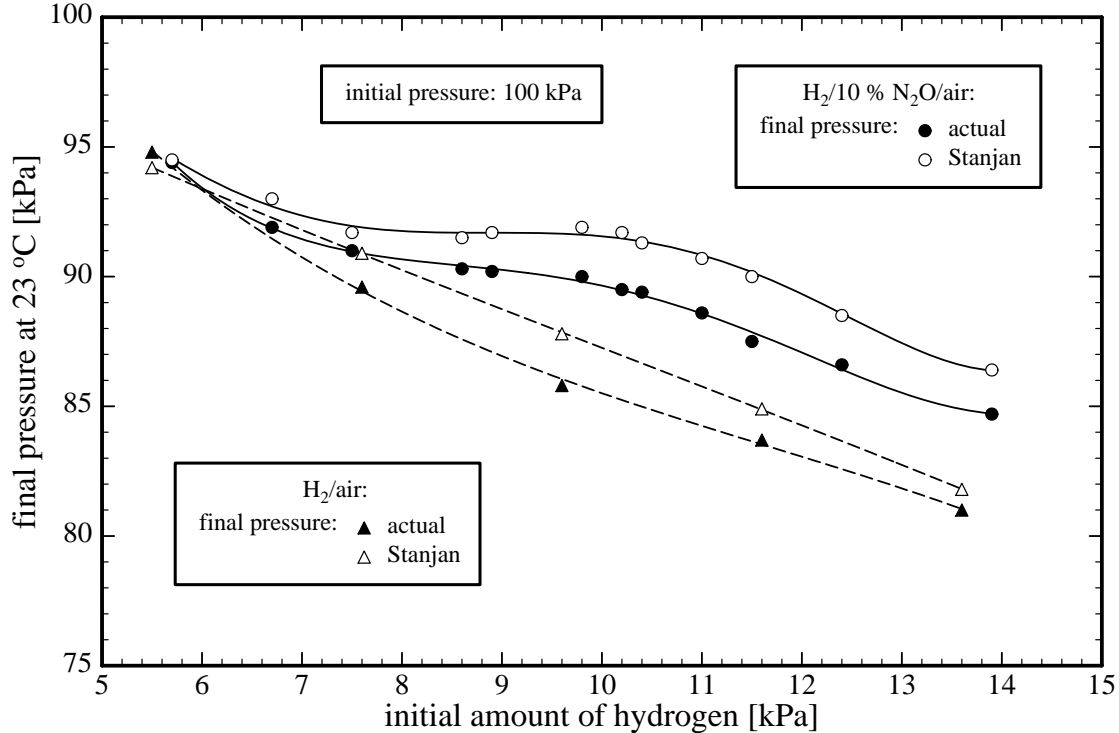
Figure 20: Final pressure. Comparison between post-burn measurements and STANJAN calculations.

Run No.	initial CH_4 [kPa]	initial N_2O [kPa]	final N_2O [kPa]	final CH_4 [kPa]	final pressure [kPa]	peak pressure bar
259	4.5	10.1	10.0	4.5	-	-
260	4.8	10.1	0.35	0.0	95.4	5.97
258	4.9	10.0	0.35	0.0	95.3	6.16
257	5.9	10.05	0.25	0.0	93.2	4.90
256	7.9	10.05	0.25	0.0	90.6	8.09
255	10.0	10.05	0.3	0.4	87.7	9.20

Table 10: Initial and final gas composition, actual final and peak pressure of CH_4–N_2O–air runs.
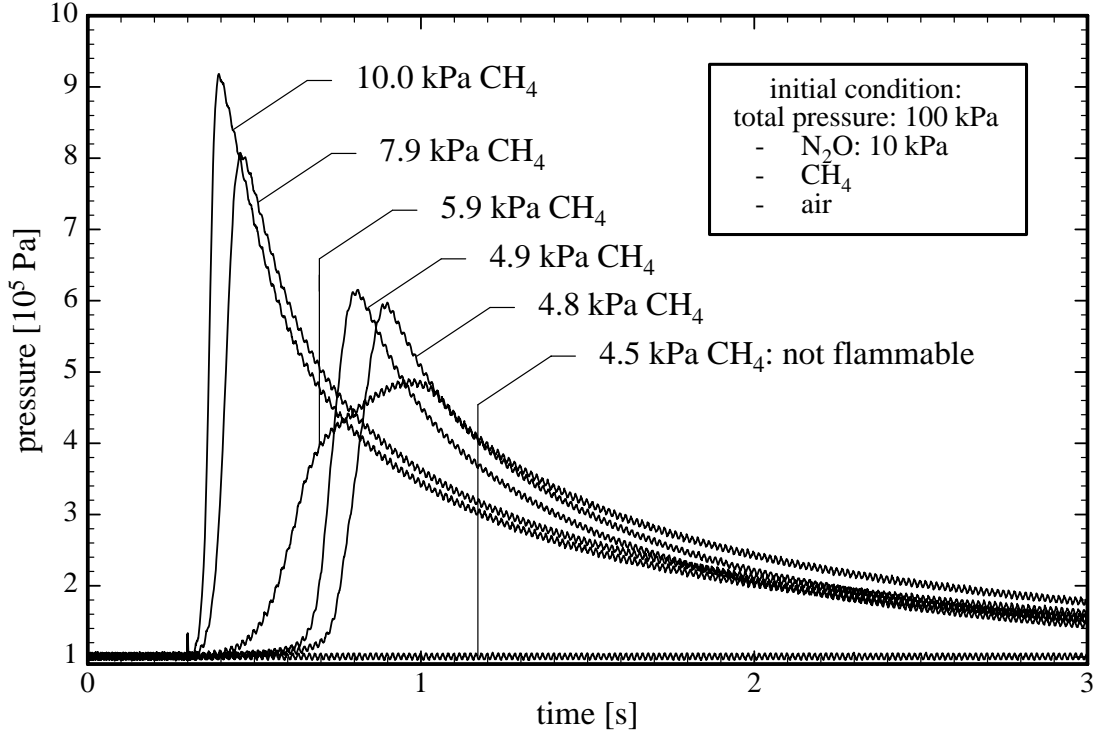
Figure 21: Combustion pressure histories of methane–nitrous oxide–air mixtures.

4.2   Methane–Nitrous Oxide–Air Mixtures

For these investigations, the initial gas partial pressure of methane was varied from 4.5 to 10.0 kPa, and the initial partial pressure of nitrous oxide was nominally 10 kPa. Figure 21 shows the pressure histories for these tests, in which the pressure peak increases with increasing CH_4 concentration from 5.9 bar (4.8 kPa CH_4) over 6.1 bar (4.9 kPa CH_4) and 8.1 bar (7.9 kPa CH_4) to 9.2 bar (10.0 kPa CH_4). The values of initial and final gas partial pressures of CH_4 and N_2O and of peak pressures of the CH_4–N_2O–air runs are shown in Table 10. The pressure history for 5.9 kPA CH_4 is atypical and should not be used in analysis.

Figure 22 shows the results of the nitrous oxide consumption during methane–nitrous oxide–air mixture combustion. The results are very different from the results of hydrogen–nitrous oxide–air mixtures presented above. If the mixture is flammable, the nitrous oxide is almost totally consumed. For initial methane amounts above 4.8 kPa the final amount of nitrous oxide varies between 0.25 and 0.35 kPa and the final amount of methane is below 0.4 kPa. For 4.5 kPa initial methane, the mixture is not flammable and therefore no methane or nitrous oxide is consumed. Compared to H_2–N_2O–air mixtures the heat of combustion of

19
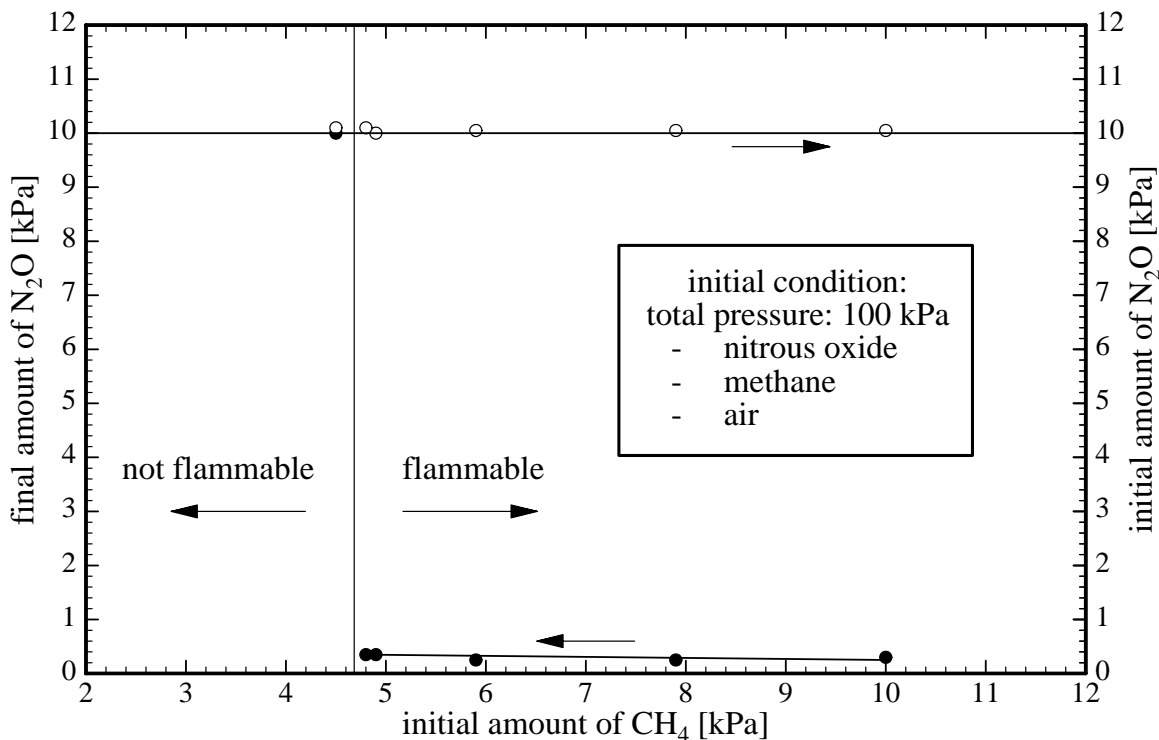
Figure 22: Nitrous oxide consumption in methane–nitrous oxide–air combustion.

CH_4–N_2O–air mixtures is higher. Therefore, the flame temperature at the flammability limit will be much higher for CH_4 than in the case of H_2. It follows that the rate of thermal decomposition of N_2O

$$N_2O + (M) \rightarrow N_2 + O + (M)$$
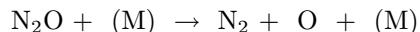
with an Arrhenius activation energy of around 60 kcal/mole (Breshears 1995) will still be high enough at the CH_4 LFL and decomposition will always occur. This is also observed for NH_3 (Ross and Shepherd 1996), with significant N_2O decomposition occurring near the lean limit of mixtures containing large fractions of NH_3.

4.3 Ammonia–Nitrous Oxide Mixtures

For these investigations, the initial gas partial pressure of ammonia was varied from 4.5 to 8.0 kPa at 0 kPa nitrogen dilution and from 10 to 11 kPa at 54 kPa nitrogen dilution. In contrast to the hydrogen and methane investigations the fuel–oxidizer mixtures did not contain air, the only oxidizer was nitrous oxide. The values of initial gas partial pressures of NH_3, N_2O and N_2, of final partial pressures of N_2O and of actual final and peak pressures of the NH_3–N_2O–N_2 runs are shown in tables 11 and 12.

Figures 23 and 24 show the results of the nitrous oxide consumption during ammonia–nitrous oxide mixture combustion at 0 and 54 kPa nitrogen dilution. The results are very different from the results of hydrogen–nitrous oxide–air mixtures and very similar to the results of methane–nitrous oxide–air mixtures presented above. If the mixture is flammable, the nitrous oxide is almost totally consumed.

Run No.	initial NH$_3$ [kPa]	initial N$_2$O [kPa]	final N$_2$O [kPa]	final pressure [kPa]	peak pressure bar
456a	4.5	95.5	95.5	-	-
457	5.0	95.0	95.0	-	-
629	5.2	94.8	0.77	137.3	11.5
522a	7.0	93.0	0.66	135.0	11.5
528	8.0	92.0	0.65	133.2	11.8

Table 11: Initial and final gas composition, actual final and peak pressure of NH$_3$–N$_2$O runs.

Run No.	initial NH$_3$ [kPa]	initial N$_2$O [kPa]	initial N$_2$ [kPa]	final N$_2$O [kPa]	final pressure [kPa]	peak pressure bar
496	10.0	36.0	54.0	35.5	-	-
553	10.9	35.1	54.0	35.0	-	-
630	11.0	35.0	54.0	0.39	104.8	7.93

Table 12: Initial and final gas composition, actual final and peak pressure of NH$_3$–N$_2$O–N$_2$ runs (54 kPa nitrogen dilution).
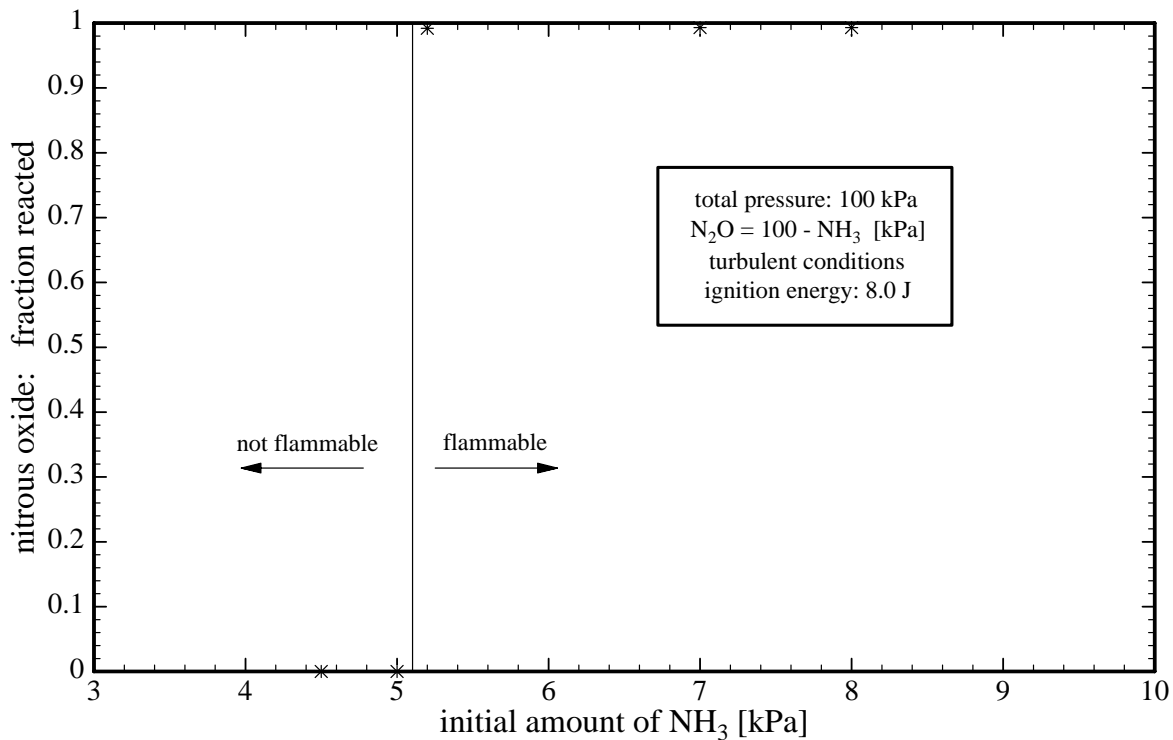
Figure 23: Nitrous oxide consumption in ammonia–nitrous oxide combustion.
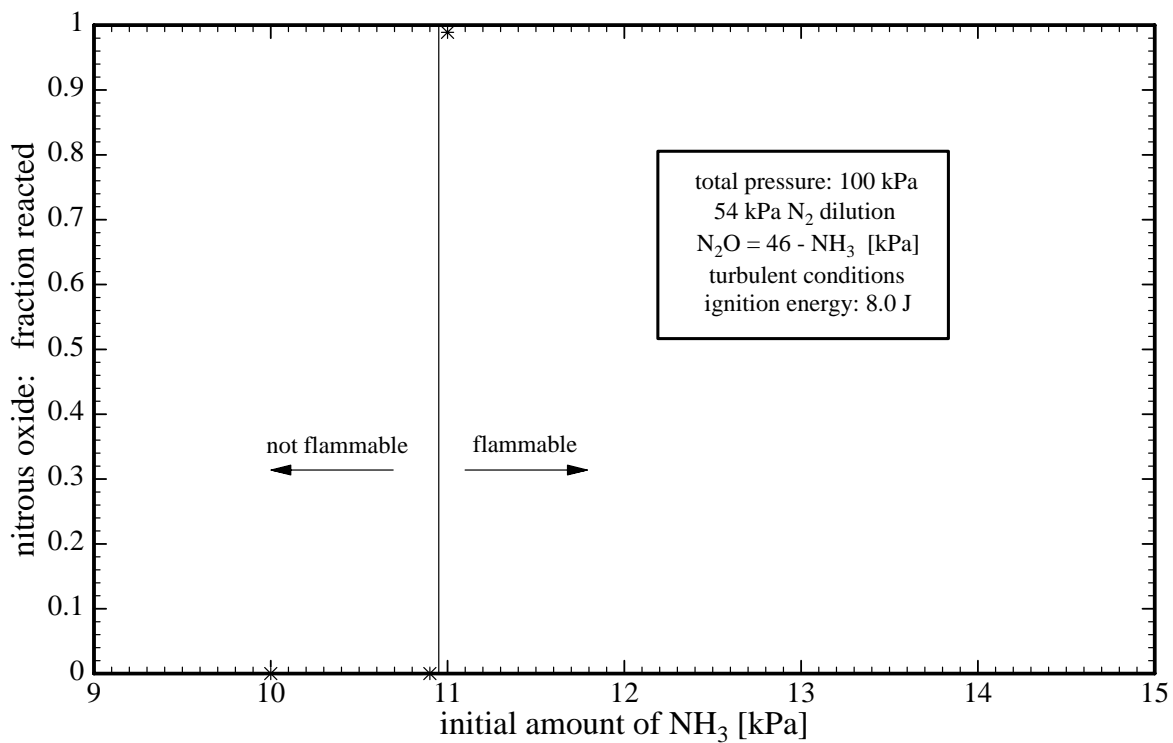
Figure 24: Nitrous oxide consumption in ammonia–nitrous oxide–nitrogen combustion.

4.4 Mixtures A/B/C/D with Air

The nitrous oxide consumption during combustion of mixture A (42% H_2, 36% N_2O, 21% NH_3, 1% CH_4), mixture B (35% H_2, 35% N_2O, 30% NH_3), mixture C (25% H_2, 25% N_2O, 50% NH_3) and mixture D (16.7% H_2, 33.3% N_2O, 50% NH_3) with air was measured around the lean flammability limits of these mixtures to verify the N_2O participation limits given in Ross and Shepherd (1996). The results are shown in Fig. 25. The Ross and Shepherd (1996) N_2O participation limits (mixture A: 13%, mixture B: 15%, mixture c: 13%, mixture d: 15%) were confirmed by the present investigations for the mixtures A, C, and D, but not for mixture B. For this mixture, the N_2O participation limit is around 13 instead of 15%.

The values of initial gas partial pressures of mixtures A–D and air, of initial and final N_2O and of actual final and peak pressures of the mixtures A–D with air runs are shown in Tables 13, 14, 15 and 16.
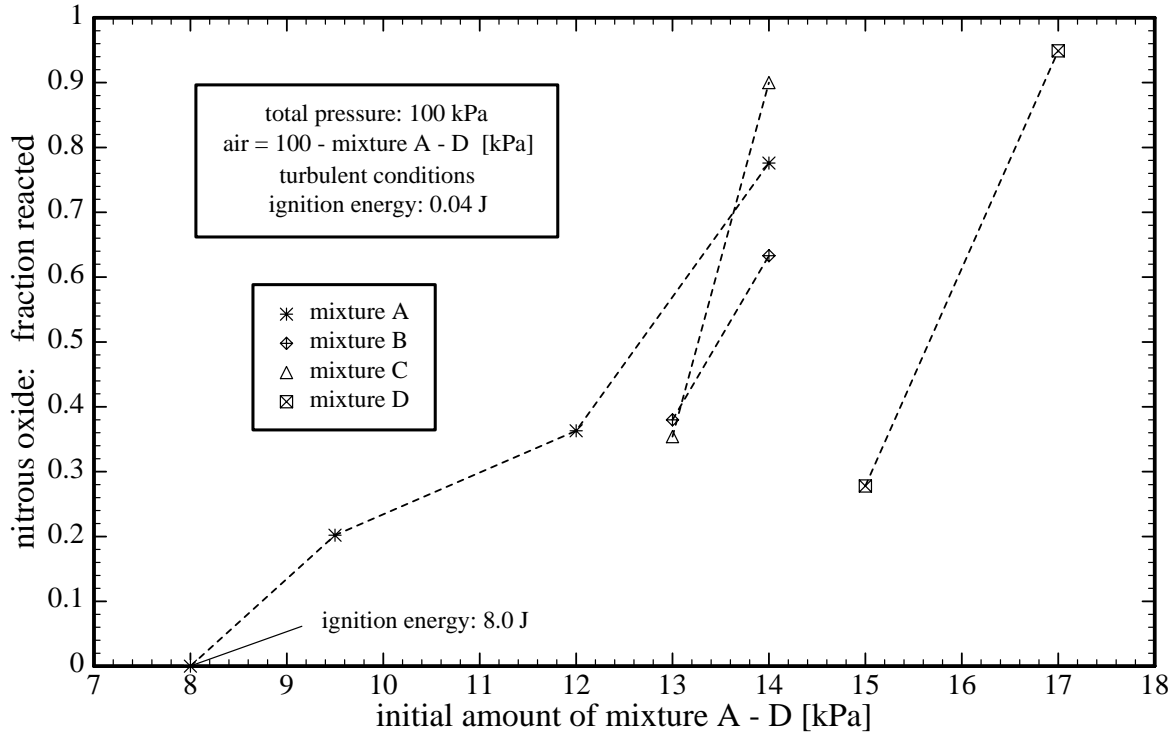
Figure 25: Nitrous oxide consumption in combustion of mixtures A-D with air.

Run No.	initial mixture a [kPa]	initial air [kPa]	initial N$_2$O [kPa]	final N$_2$O [kPa]	final pressure [kPa]	peak pressure bar
632	8.0	92.0	2.88	2.88	-	-
631	9.5	90.5	3.42	2.73	96.9	1.90
621	12.0	88.0	4.32	2.75	91.7	3.14
622	14.0	86.0	5.04	1.13	89.5	4.22

Table 13: Initial and final gas composition, actual final and peak pressure of mixture A–air runs.

Run No.	initial mixture b [kPa]	initial air [kPa]	initial N$_2$O [kPa]	final N$_2$O [kPa]	final pressure [kPa]	peak pressure bar
624	13.0	87.0	4.55	2.82	86.9	3.48
623	14.0	86.0	4.90	1.80	93.6	3.96

Table 14: Initial and final gas composition, actual final and peak pressure of mixture B–air runs.

Run No.	initial mixture c [kPa]	initial air [kPa]	initial N$_2$O [kPa]	final N$_2$O [kPa]	final pressure [kPa]	peak pressure bar
625	13.0	87.0	3.25	2.10	91.1	3.51
626	14.0	86.0	3.50	0.35	87.5	4.53

Table 15: Initial and final gas composition, actual final and peak pressure of mixture C–air runs.

Run No.	initial mixture d [kPa]	initial air [kPa]	initial N$_2$O [kPa]	final N$_2$O [kPa]	final pressure [kPa]	peak pressure bar
627	15.0	85.0	5.00	3.61	94.0	3.06
628	17.0	83.0	5.67	0.29	93.6	-

Table 16: Initial and final gas composition, actual final and peak pressure of mixture D–air runs.

5 Hydrogen–Nitrous Oxide–Nitrogen Mixtures

Numerous flammability studies have been conducted with hydrogen. Some of these studies, Smith and Linnett (1953), Posthumus (1930), van der Wal (1934), and Scott et al. (1957) have been carried out with N_2O as the oxidizer. The available data are shown in Fig. 26 together with the flammability limits of hydrogen–oxygen (Coward and Jones 1952) and hydrogen–air–nitrogen mixtures (Zabetakis 1965; Shebeko et al. 1995). These data are all nominally obtained at at 25°C and 1 atm pressure. Not shown on this diagram are the H_2-N_2O-air mixture data of Cashdollar et al. (1992) and Ross and Shepherd (1996). Note that the rich limit data of Posthumus are substantially below those of Smith and Linnett. This is apparently due to the low temperature/energy ignition source of Posthumous in comparison to the 20 J spark discharge used by Smith and Linnett. In general, ignition energy has a strong effect on flammablility limits in mixtures containing large amounts of N_2O. The particular problem of ignition of very lean H_2-N_2O mixtures is discussed subsequently in Section 6.3.
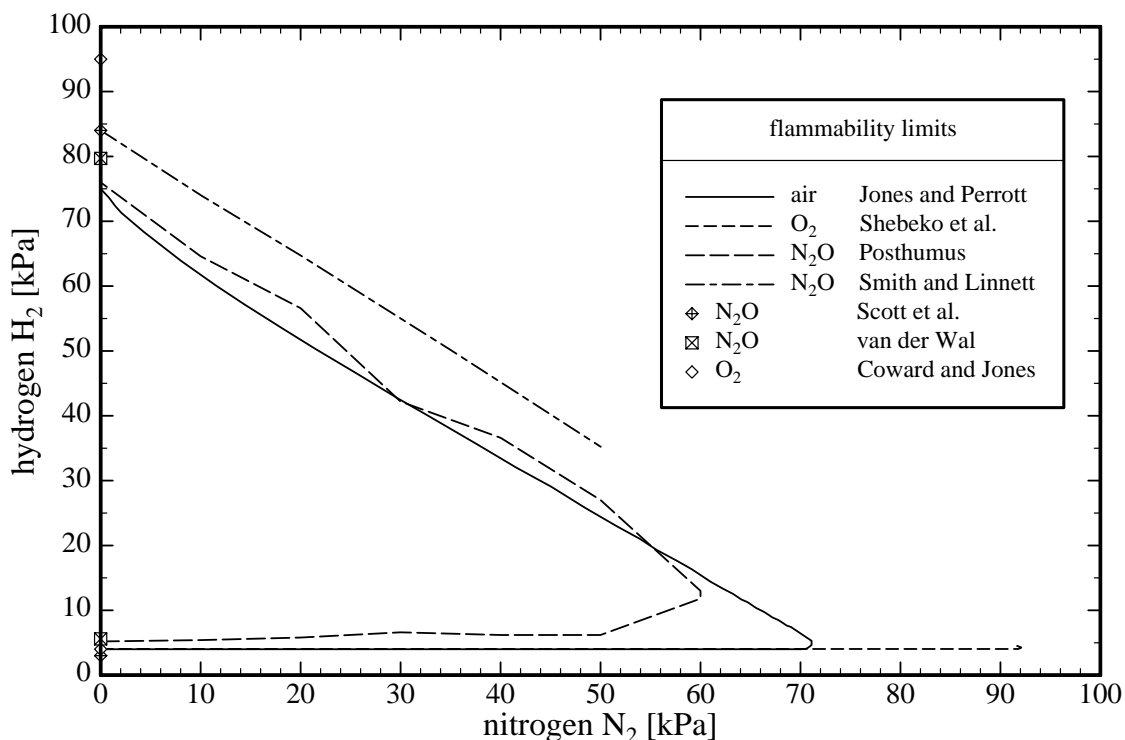
Figure 26: Flammability limits of hydrogen–air–nitrogen, hydrogen–nitrous oxide and hydrogen–oxygen–nitrogen mixtures.

6   Methane–Nitrous Oxide–Nitrogen Mixtures

Measurements with methane–nitrous oxide–nitrogen mixtures were carried out to determine the flammability limits and ignition energy bounds. Additional tests with methane–nitrous oxide–oxygen–nitrogen mixtures were done to investigate the influence of small amounts of oxygen on the flammability limit.

6.1   Flammability Limit

Flammability limits were determined for CH_4–N_2O–N_2 mixtures at a total initial pressure of 100 kPa. The ignition source was the capacitor discharge unit described in Ross and Shepherd (1996), which has a maximum electrical energy of 8 J.
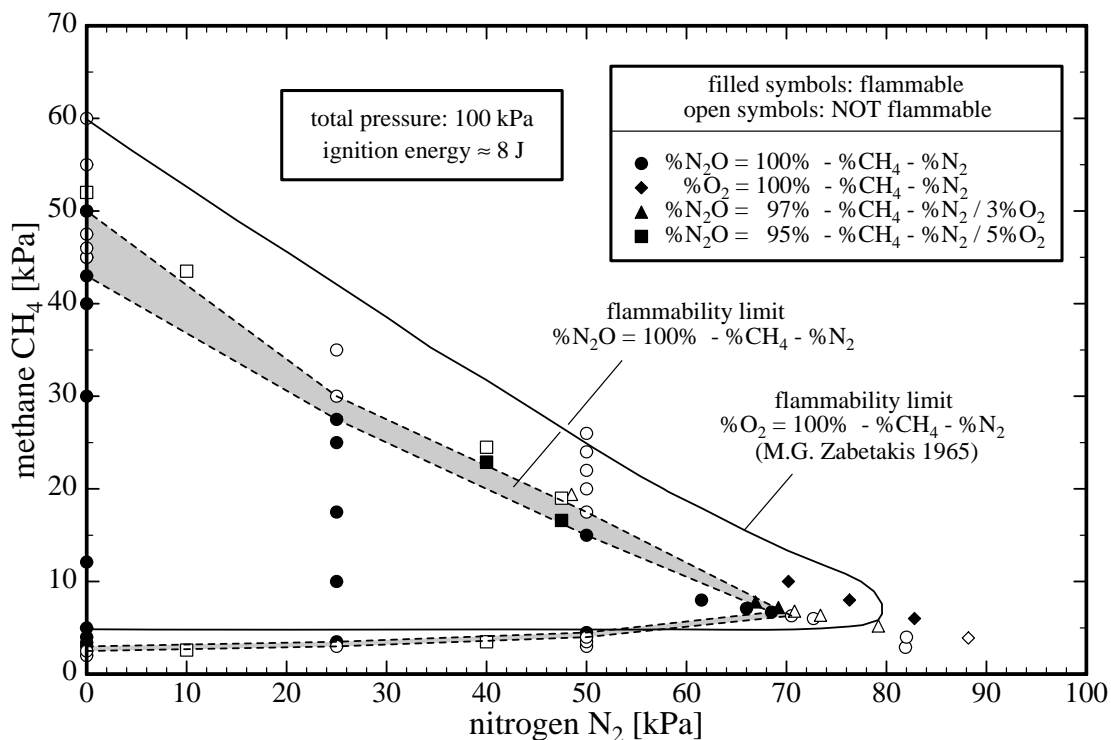
Figure 27: Flammability limits of methane–nitrous oxide–nitrogen, methane–oxygen–nitrogen and methane–nitrous oxide–oxygen–nitrogen mixtures.

The present results are shown in Fig. 27 and compared to previous results from the literature (Zabetakis 1965) for CH_4–O_2–N_2 mixtures. Previous results for CH_4–N_2O or CH_4–N_2O–N_2 mixtures were not available from the literature. The lower flammability limit shows a very smooth dependence (increase) on the amount of nitrogen dilution and a good correspondence to Zabetakis' results for CH_4–O_2–N_2, whereas the upper limit shifts to a smaller flammability region compared to CH_4–O_2–N_2 and shows a strong decrease with increasing nitrogen dilution. Without dilution, methane–nitrous oxide mixtures are flammable for methane partial pressures between 2.7 and 43-50 kPa. Mixtures with nitrogen dilution above 70.5 kPa are not flammable (inert). The corresponding methane partial pressure is 6.3 kPa. The values of initial gas composition, final and peak pressure of the present CH_4–N_2O–N_2, CH_4–O_2–N_2 and CH_4–N_2O–N_2–O_2 runs are shown in Tables 17 and 18.

26

Run No.	initial CH$_4$ [kPa]	initial N$_2$O [kPa]	initial N$_2$ [kPa]	initial O$_2$ [kPa]	final pressure [kPa]	peak pressure bar
261	12.0	88.0	0.0	-	102.0	16.0
262	3.0	17.0	80.0	-	-	-
263	4.0	16.0	80.0	-	-	-
264	6.0	24.0	70.0	-	-	-
265	8.0	32.0	60.0	-	101.8	10.1
266	7.0	28.0	65.0	-	101.6	9.1
276	6.6	26.4	67.0	-	102.1	8.7
277	6.2	24.8	69.0	-	-	-
288	5.0	95.0	-	-	136.8	13.5
289	4.0	96.0	-	-	136.8	12.8
290	3.4	96.6	-	-	140.1	12.6
291	2.0	98.0	-	-	-	-
292	3.0	97.0	-	-	142.0	12.2
293	2.5	97.5	-	-	-	-
294	3.0	72.0	25.0	-	-	-
295	3.5	71.5	25.0	-	126.5	10.4
296	3.0	47.0	50.0	-	-	-
297	3.5	46.5	50.0	-	-	-
298	4.0	46.0	50.0	-	-	-
299	4.5	45.5	50.0	-	112.2	8.9
300	26.0	24.0	50.0	-	-	-
302	24.0	26.0	50.0	-	-	-
303	22.0	28.0	50.0	-	-	-
304	20.0	30.0	50.0	-	-	-
309	50.0	50.0	-	-	173.2	13.4
310	60.0	40.0	-	-	-	-
311	55.0	45.0	-	-	-	-
312	35.0	40.0	25.0	-	-	-
313	45.0	55.0	-	-	-	-
314	10.0	65.0	25.0	-	113.5	13.4
315	40.0	60.0	-	-	165.9	14.6
316	30.0	45.0	25.0	-	-	-
317	45.0	55.0	-	-	-	-
318	25.0	50.0	25.0	-	130.8	13.4
319	30.0	70.0	-	-	112.2	17.1
320	50.0	50.0	-	-	167.6	14.1
321	15.0	35.0	50.0	-	115.6	10.1
322	20.0	30.0	50.0	-	-	-
325	17.5	32.5	50.0	-	-	-
327	17.5	57.5	25.0	-	108.2	14.4
328	27.5	47.5	25.0	-	139.7	12.1
335	47.5	52.5	-	-	-	-
336	46.0	54.0	-	-	-	-
337	43.0	57.0	-	-	170.4	12.1

Table 17: Initial gas composition, actual final and peak pressure of CH$_4$–N$_2$O–N$_2$ runs.

Run No.	initial CH$_4$ [kPa]	initial N$_2$O [kPa]	initial N$_2$ [kPa]	initial O$_2$ [kPa]	final pressure [kPa]	peak pressure bar
267	10.0	-	70.0	20.0	82.2	8.4
268	8.0	-	76.0	16.0	85.9	7.5
269	6.0	-	82.0	12.0	94.4	5.7
270	4.0	-	88.0	8.0	-	-
271	5.0	14.0	78.0	3.0	-	-
272	6.2	18.8	72.0	3.0	-	-
273	7.6	24.4	65.0	3.0	99.4	9.1
274	7.0	22.0	68.0	3.0	99.4	8.4
275	6.5	20.2	70.3	3.0	-	-
323	19.4	29.1	48.5	3.0	-	-
324	19.0	28.5	47.5	5.0	-	-
326	16.6	30.9	47.5	5.0	111.3	10.7
329	52.0	43.0	-	5.0	-	-
330	2.6	82.4	10.0	5.0	-	-
331	3.5	51.5	40.0	5.0	-	-
332	22.9	32.1	40.0	5.0	127.3	10.2
333	24.5	30.5	40.0	5.0	-	-
334	43.5	41.5	10.0	5.0	-	-

Table 18: Initial gas composition, actual final and peak pressure of CH$_4$–O$_2$–N$_2$ and CH$_4$–N$_2$O–N$_2$–O$_2$ runs.

6.2 Influence of Small Amounts of Oxygen (3 - 5%) on the Flammability Limit

Figures 27 and 28 show no pronounced dependence of the flammability limits of methane–nitrous oxide–nitrogen mixtures on small amounts of oxygen. At 3 kPa oxygen addition, the maximum flammable nitrogen dilution does not shift (see Fig. 28). Substituting oxygen for nitrous oxide shifts the maximum flammable nitrogen dilution (inerting concentration) from 70.5 to about 85 kPa (5 kPa CH$_4$ and 10 kPa O$_2$). Zabetakis obtained 80 kPa nitrogen dilution as the inerting concentration for CH$_4$–O$_2$–N$_2$ mixtures at atmospheric pressure and 26°C (Zabetakis 1965). The present results exceed this value due to turbulent conditions (the mixing fan was on during the burn). Addition of 5 kPa oxygen at 0, 10, 40 and 47.5 kPa nitrogen dilution does not appreciably alter the flammability limit (see Fig. 27).

6.3 Influence of Ignition Energy on the Flammability Limit

It is known that (Kuchta 1985) the minimum ignition energy is a strong function of composition near the flammability limit. The minimum value of ignition energy for hydrocarbon fuels in air occurs for for rich mixtures and is typically on the order of 0.25 mJ. Near the limits, a steep rise in minimum ignition energy is observed, with mixtures outside the flammability limit exhibiting inert behavior even for very large amounts of energy.

We determined bounds on the ignition energy by carrying out a series of tests with ignition energies of 0.04, 0.2, 1.0, 2.0, 5.0 and 8.0 J. For each ignition energy, the minimum amount of methane for flammability of a methane–nitrous oxide mixture at 100 kPa (no nitrogen dilution) was determined.

The results of these runs are shown in Table 19 and plotted in Figs. 29 and 30. Figure 29 shows the peak pressures compared to peak pressures resulting from STANJAN calculations. At the leanest flammable concentration (2.8% CH$_4$), the peak pressure is about 12 bar, close to the value obtained from N$_2$O decomposition alone (11.8 bar). This behavior is similar to that observed for H$_2$-N$_2$O mixtures by Cashdollar et al. (1992), who found that with sufficient ignitor energy (5000 J), mixtures with as little as 1% H$_2$ could be ignited. Their limiting fuel concentration with a 58 J spark was about 6% H$_2$ for downward propagation.

Run No.	initial CH$_4$ [kPa]	initial N$_2$O [kPa]	ignition energy [J]	final pressure [kPa]	peak pressure bar
338	4.0	96.0	0.04	-	-
338a	4.0	96.0	0.2	140.0	12.7
339	5.0	95.0	0.04	130.3	13.2
340	4.5	95.5	0.04	-	-
340a	4.5	95.5	0.2	143.4	13.0
341	4.75	95.25	0.04	136.4	13.0
342	4.25	95.75	0.04	-	-
342a	4.25	95.75	0.2	136.6	12.8
343	3.75	96.25	0.04	-	-
343a	3.75	96.25	0.2	142.3	12.6
344	3.5	96.5	0.2	140.5	12.3
345	3.25	96.75	0.2	142.0	12.1
346	3.0	97.0	0.2	140.3	11.9
347	2.9	97.1	0.2	140.0	11.9
348	2.8	97.2	0.2	-	-
348a	2.8	97.2	1.0	142.5	11.8
349	2.7	97.3	1.0	141.8	11.8
350	2.6	97.4	1.0	-	-
350a	2.6	97.4	2.0	-	-
350b	2.6	97.4	5.0	-	-
350c	2.6	97.4	8.0	132.1	6.05
293	2.5	97.5	8.0	-	-

Table 19: Initial gas composition, ignition energy, actual final and peak pressure of CH$_4$–N$_2$O runs.
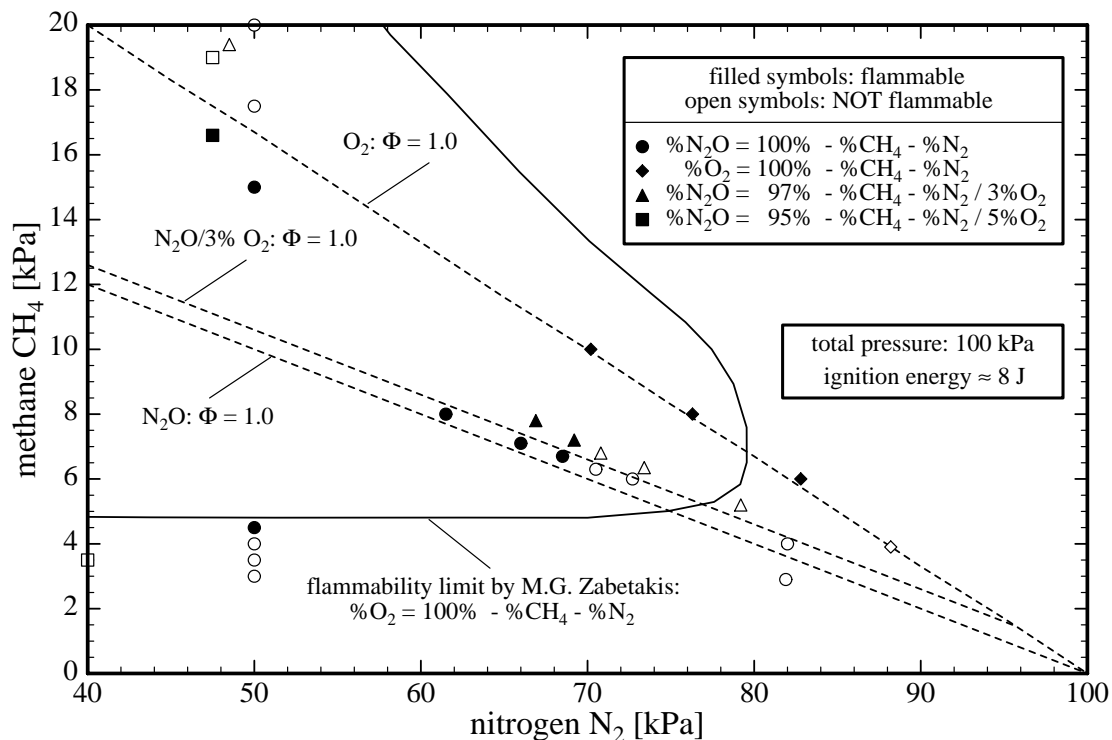
Figure 28: Influence of small amounts of oxygen on the flammability limit of methane–nitrous oxide–nitrogen mixtures.

Hertzberg and Zlochower (1993) propose that H-atoms catalyze N_2O decomposition and compounds such as H_2, CH_4 and NH_3 will, in small amounts (1-2%), accelerate the decomposition reaction sufficiently to stabilize the propagation of a decomposition flame. Substantial N_2O decomposition and associated high pressures have been observed for H_2, CH_4 and NH_3, the last being discussed by Jones and Kerr (1949). Note that pressures are really not "high" but simply close to the 12 bar value that results from N_2O decomposition. These values seemed high to previous investigators who were used to modest pressures for near-limit combustion of hydrocarbon-air mixtures. It was common practice (and still is) to investigate flammability limits in hydrocarbon-air mixtures with a glass apparatus. The destruction of these experiments when investigating N_2O alarmed these invetigators but in hindsight it is a natural consequence of working with large amounts of N_2O.

Figure 30 shows the minimum ignition energy as a function of methane concentration near the flammability limit. These results show that for ignition energies above about 1.0 J, the flammability limit is independent of the ignition energy. Increasing the ignition energy from 40 mJ to 8 J reduces the ignition limit from 2.8 to 4.8% CH_4. Similar reductions in the LFL of H_2 have been obtained in H_2-N_2O-air mixtures by Cashdollar et al. (1992). However, experiments (Cashdollar et al. 1992) using pyrotechnic ignitors and H_2-N_2O mixtures have shown that if the ignitor energy content is increased by several orders of magnitude (up to 5,000-10,000 J), then decomposition flames can be produced even (Hertzberg and Zlochower 1993) in the absence of any fuel!

We propose that the behavior of lean fuel-N_2O mixtures can be divided into two regimes: 1) low-to-moderate ignition energy (up to 100 J); 2) high ignition energy (above 5000 J). For the low-to-moderate energy regime, there is a well-defined minimum concentration of fuel (LFL) independent of ignition energy up to some value, at least 100 J. For the high-energy regime, decomposition reactions can be initiated irrespective of the amount of fuel as long as the energy is released rapidly enough. The precise details of the chemical and physical mechanism are not well understood at present but for the purposes of most safety assessments, it is probably sufficient to characterize the behavior in the low-to-moderate energy regime. It
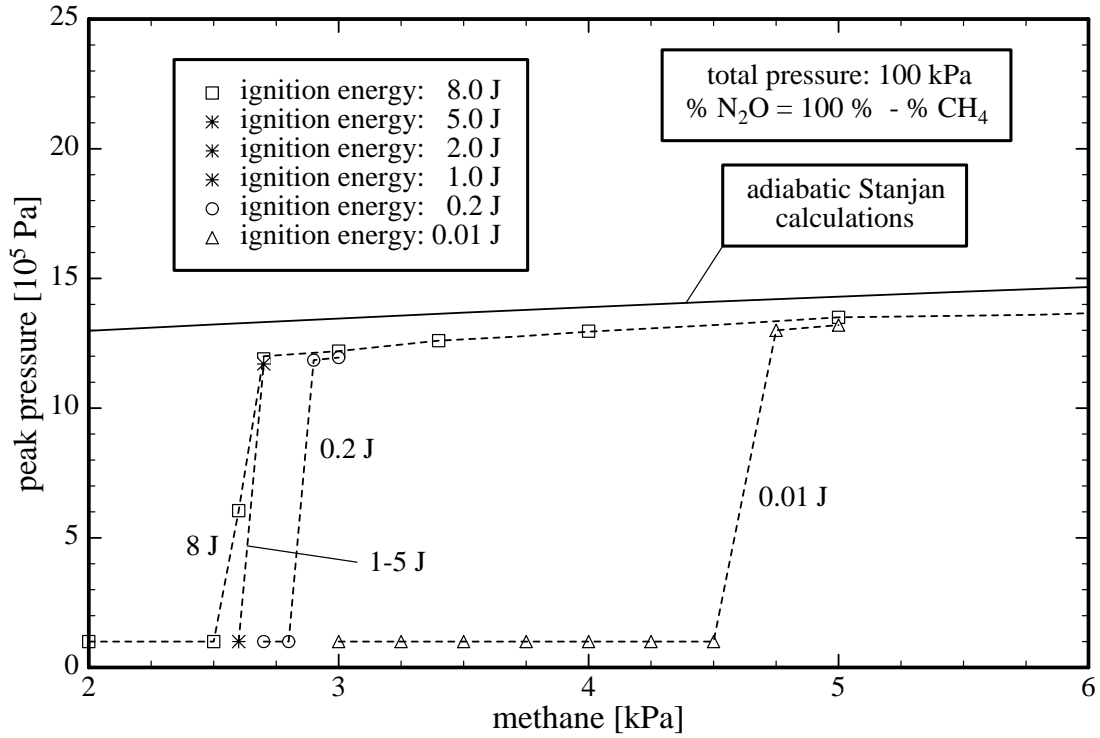
Figure 29: Peak pressure vs. methane concentration for various ignition energies.
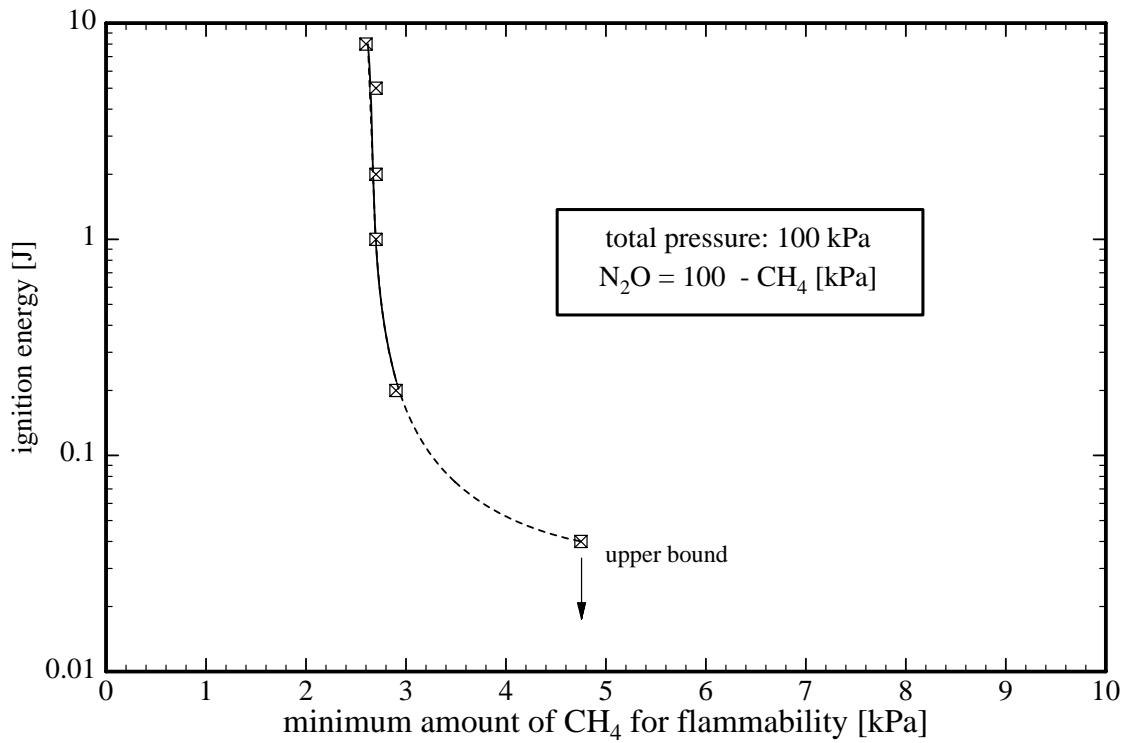
Figure 30: Minimum ignition energy as a function of methane concentration.

remains an intriguing problem in combustion science to determine the details of the flame initiation and propagation in very lean fuel-N_2O mixtures.

7   Ammonia–Nitrous Oxide–Nitrogen Mixtures

Previous investigations of lean combustion characteristics of hydrogen–nitrous oxide–ammonia mixtures in air are described in Ross and Shepherd (1996). That work focused on the lean flammability limit behavior of NH_3 and four selected H_2-N_2O-NH_3 blends (mixtures A - D) in air. Peak and final pressures were used to infer N_2O participation. Pressure measurements and visual observations were used to determine LFL values for upward and downward flame propagation (see Chapter 4.4). Increasing amounts of N_2O resulted in decreasing the LFL but only modest amounts of N_2O were examined.

Flammability studied have been conducted with ammonia by Fenton et al. (1995), Armitage and Gray (1965), Andrews and Gray (1964), Buckley and Husa (1962), van der Wal (1934), Jorissen and Ongkiehong (1926) and White (1922). We have made measurements with ammonia–nitrous oxide–nitrogen and ammonia–nitrous oxide–air mixtures to determine lower and upper flammability limits and inerting concentrations. Furthermore, ignition energy bounds without dilution and near the inerting concentration of nitrogen were investigated.

7.1   Flammability Limit

Flammability limits were determined for NH_3–N_2O–N_2 and NH_3–N_2O–air mixtures at a total initial pressure of 100 kPa. The present results are shown in Fig. 31 with nitrogen dilution and in Fig. 32 with air dilution. The flammability limits of ammonia–nitrous oxide mixtures occur at 5.2% (LFL) and 67.5% (UFL) ammonia for ignition energies less than 10 J. Addition of 60% nitrogen (see Fig. 31) or 84% air (see Fig. 32) will inert the mixtures.

Figure 31: Flammability limits of ammonia–nitrous oxide–nitrogen mixtures.

All relevant values of initial gas composition, final and peak pressure of the present NH_3–N_2O, NH_3–N_2O–N_2 and NH_3–N_2O–air mixtures are given in the Tables 20, 21 and 22.

Figure 32: Flammability limits of ammonia–nitrous oxide–air mixtures.

Run No.	initial NH$_3$ [kPa]	initial N$_2$O [kPa]	final pressure [kPa]	peak pressure bar
455	7.0	93.0	137.5	11.8
456	3.0	97.0	-	-
457	5.0	95.0	-	-
458	6.0	94.0	137.6	11.75
459	71.0	29.0	-	-
460	68.0	32.0	-	-
461	65.0	35.0	130.7	11.0
462	67.0	33.0	131.8	10.1
463	67.5	32.5	129.8	9.6
464	5.5	94.5	137.1	11.45

Table 20: Initial gas composition, actual final and peak pressure of NH$_3$–N$_2$O runs.

Run No.	initial NH$_3$ [kPa]	initial N$_2$O [kPa]	initial N$_2$ [kPa]	final pressure [kPa]	peak pressure bar
465	10.0	25.0	65.0	-	-
466	10.5	29.5	60.0	-	-
467	8.9	36.1	55.0	-	-
468	8.5	38.7	52.8	-	-
469	7.7	44.8	47.5	-	-
470	20.0	50.0	30.0	102.1	11.7
471	20.0	40.0	40.0	97.8	10.7
472	18.0	27.0	55.0	93.9	9.2
473	16.0	24.0	60.0	94.9	8.1
474	15.6	23.4	61.0	-	-
475	16.4	24.6	59.0	95.0	8.2
476	14.8	22.2	63.0	-	-
477	20.2	20.8	59.0	-	-
478	14.0	27.0	59.0	98.1	8.4
479	8.0	74.0	18.0	124.2	10.5
481	7.0	75.0	18.0	124.3	10.2
482	6.0	76.0	18.0	-	-
483	6.5	75.5	18.0	-	-
484	52.0	30.0	18.0	119.5	9.6
485	56.0	26.0	18.0	-	-
486	54.0	28.0	18.0	-	-
487	53.0	29.0	18.0	-	-
488	52.5	29.5	18.0	-	-
489	37.0	27.0	36.0	-	-
490	35.0	29.0	36.0	108.9	9.8
491	36.0	28.0	36.0	109.5	9.4
492	9.0	55.0	36.0	113.9	9.0
493	8.0	56.0	36.0	-	-
494	8.5	55.5	36.0	-	-
495	11.0	35.0	54.0	104.6	8.1
496	10.0	36.0	54.0	-	-
497	10.5	35.5	54.0	-	-
498	22.0	24.0	54.0	-	-
499	21.0	25.0	54.0	97.6	8.8
500	17.2	22.3	60.5	-	-
501	17.0	23.0	60.0	-	-
502	14.0	26.0	60.0	-	-
503	15.0	25.5	59.5	96.7	8.3
504	14.8	24.7	60.5	-	-
505	12.5	29.5	58.0	101.7	7.6
506	12.0	29.5	58.5	101.0	7.4
507	11.5	29.5	59.0	101.2	7.4
555	21.5	24.5	54.0	-	-
557	20.75	25.25	54.0	96.4	8.8
558	20.0	26.0	54.0	95.5	9.1
561	12.0	34.0	54.0	102.6	8.4
563	18.4	27.6	54.0	93.7	9.4

Table 21: Initial gas composition, actual final and peak pressure of NH$_3$–N$_2$O–N$_2$ runs.

Run No.	initial NH$_3$ [kPa]	initial N$_2$O [kPa]	initial air [kPa]	final pressure [kPa]	peak pressure bar
508	38.0	8.0	54.0	-	-
509	37.0	9.0	54.0	92.8	8.2
510	53.0	20.0	27.0	-	-
511	52.0	21.0	27.0	112.4	9.1
512	11.0	35.0	54.0	103.2	7.9
513	10.0	36.0	54.0	-	-
514	29.0	0.0	71.0	-	-
515	28.0	0.0	72.0	83.6	6.6
516	7.0	66.0	27.0	-	-
517	8.0	65.0	27.0	118.0	9.2
548	16.0	24.0	60.0	93.2	8.4
549	12.0	18.0	70.0	-	-
550	13.2	19.8	67.0	94.9	7.2

Table 22: Initial gas composition, actual final and peak pressure of NH$_3$–N$_2$O–air runs.

7.2 Influence of Ignition Energy on the Flammability Limit

The dependence of the flammability limits on ignition energy were determined for NH_3–N_2O and NH_3–N_2O–N_2 mixtures for energies between 0.04 and 8 J. For NH_3–N_2O mixtures, the value for the lower flammability limit increases from 5.2% ammonia for 8 J to 11.5% ammonia for 0.04 J (see Figs. 33, 35 and 37), whereas the value for the upper flammability limit at 0.04 J decreases to 54% (8 J: 67.5% ammonia , see Figs. 34, 36 and 37). Calcote et al. (1952) measured a minimum spark ignition energy of 0.07 mJ (see Fig. 37) for a 40% ammonia–60% nitrous oxide mixture at atmospheric pressure. Our measured ignition energy bounds at 54% nitrogen dilution are shown in Figs. 38 and 39. A stochiometric ammonia–air mixture at 100 kPa initial pressure (21.9% ammonia, 78.1% air, see Table 26) could not be ignited with energies less than 50 mJ, whereas the mixture was flammable for energies more than 100 mJ. Buckley and Husa (1962) obtained a minimum ignition energy of 680 mJ for ammonia–air mixtures.
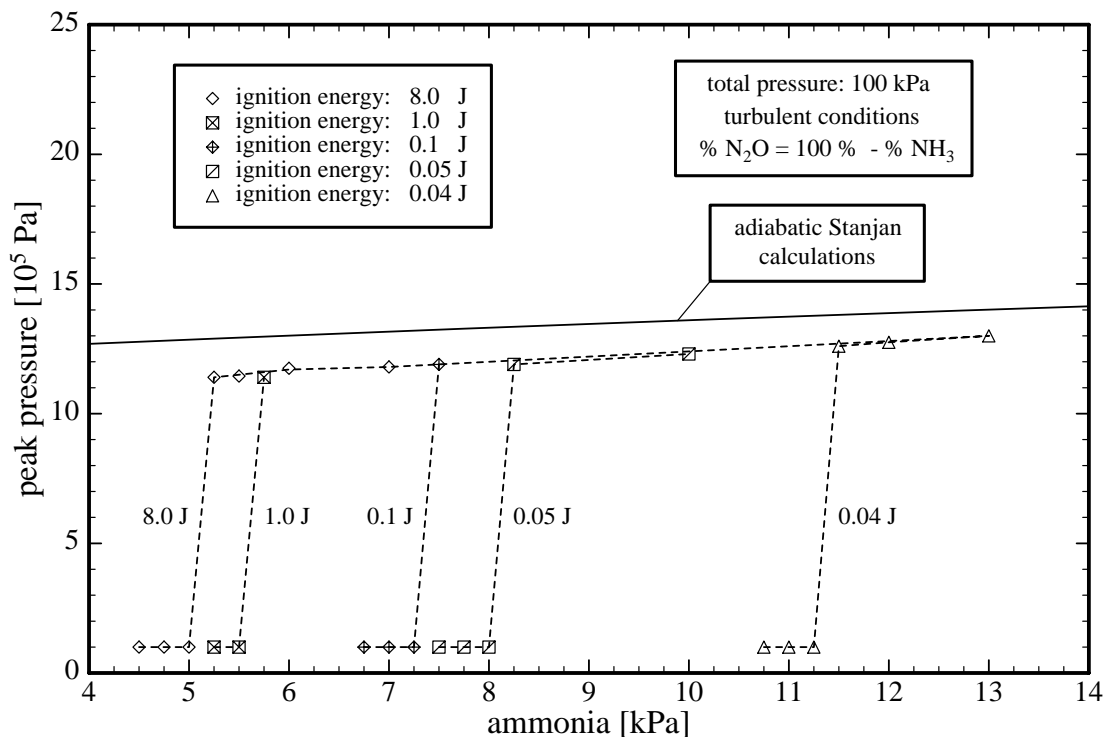

Figure 33: Peak pressure vs. ammonia concentration for various ignition energies; lower limit.

All relevant values of initial gas composition, ignition energy, final and peak pressure of the present NH_3–N_2O and NH_3–N_2O–N_2 mixtures are given in Table 23 (no dilution, lower limit), Table 24 (no dilution, upper limit) and Table 25 (54% nitrogen dilution, lower and upper limit).
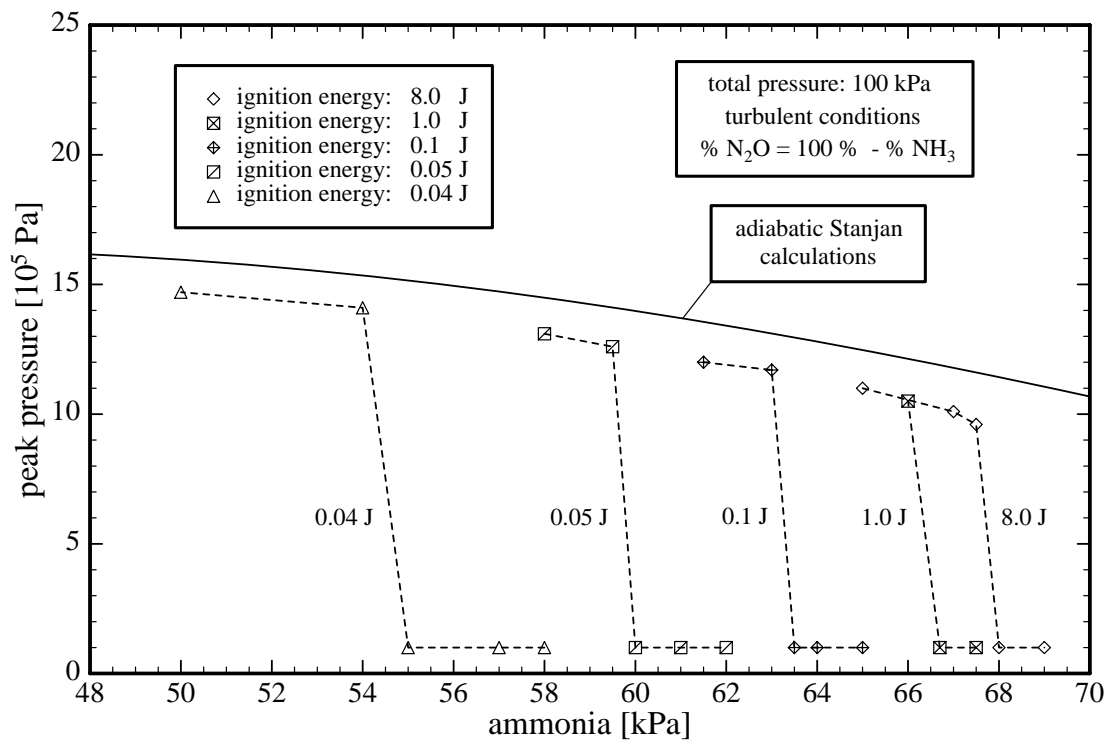
Figure 34: Peak pressure vs. ammonia concentration for various ignition energies; upper limit.

Figure 35: Minimum ignition energy as a function of ammonia concentration; lower limit.

Figure 36: Minimum ignition energy as a function of ammonia concentration; upper limit.

Figure 37: Minimum ignition energy as a function of ammonia concentration.
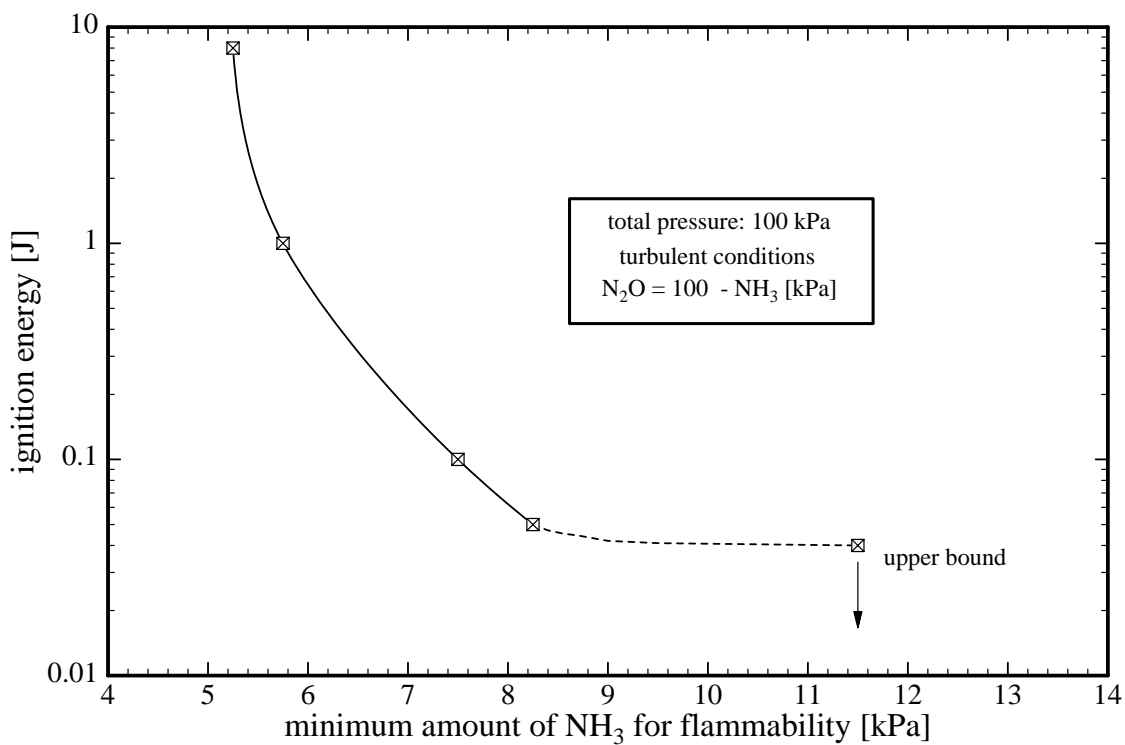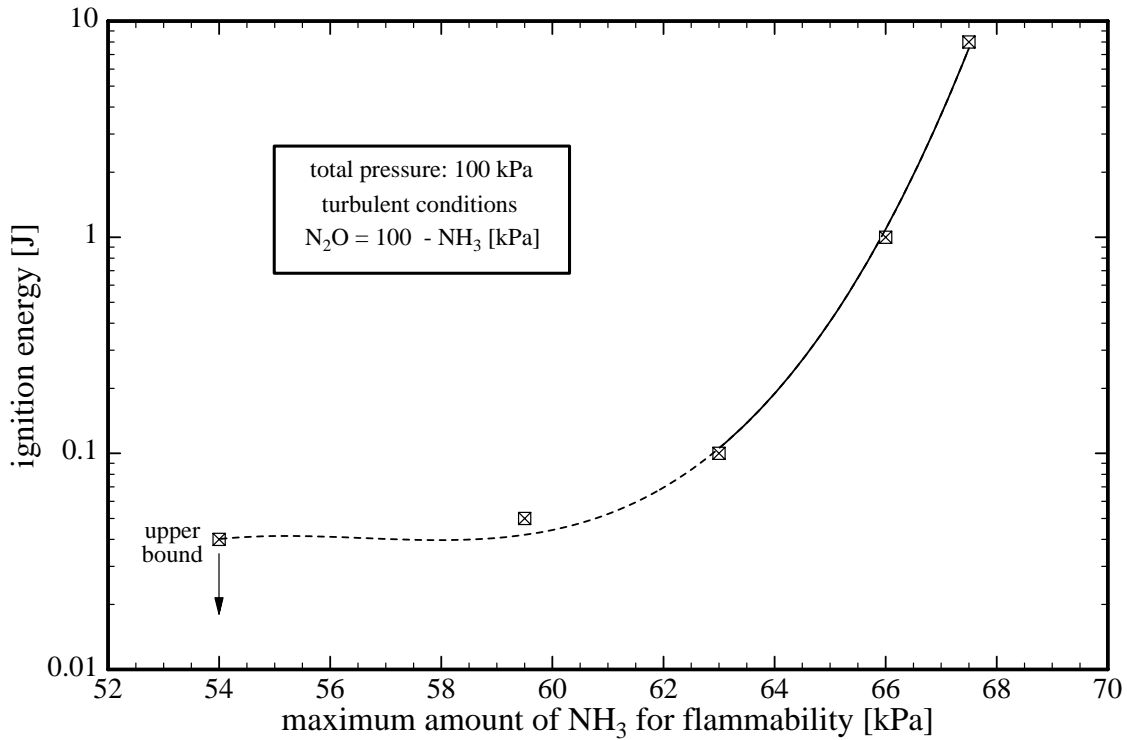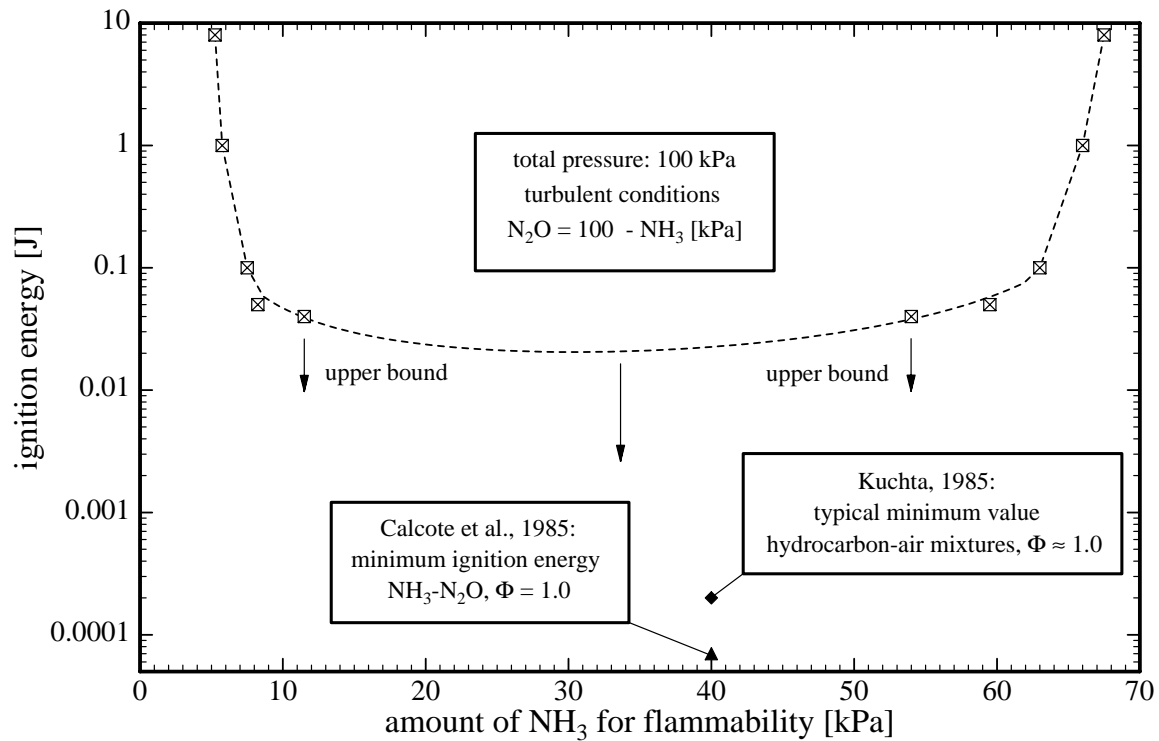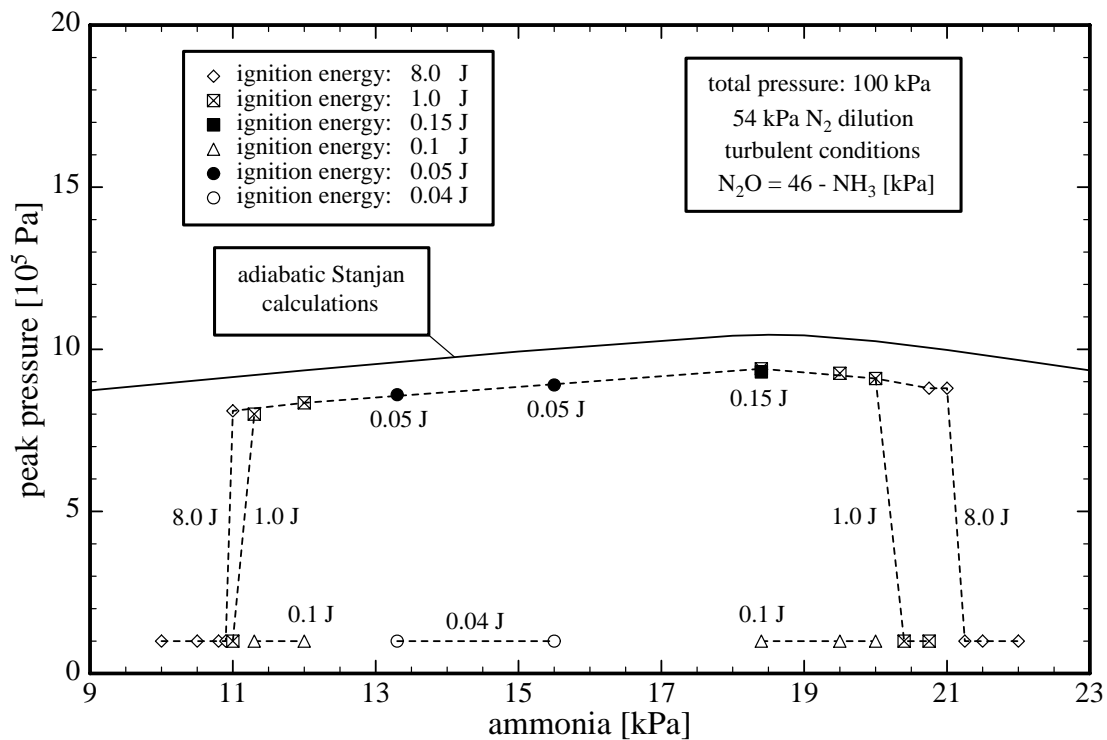
Figure 38: Peak pressure vs. ammonia concentration for various ignition energies at 54 kPa nitrogen dilution.
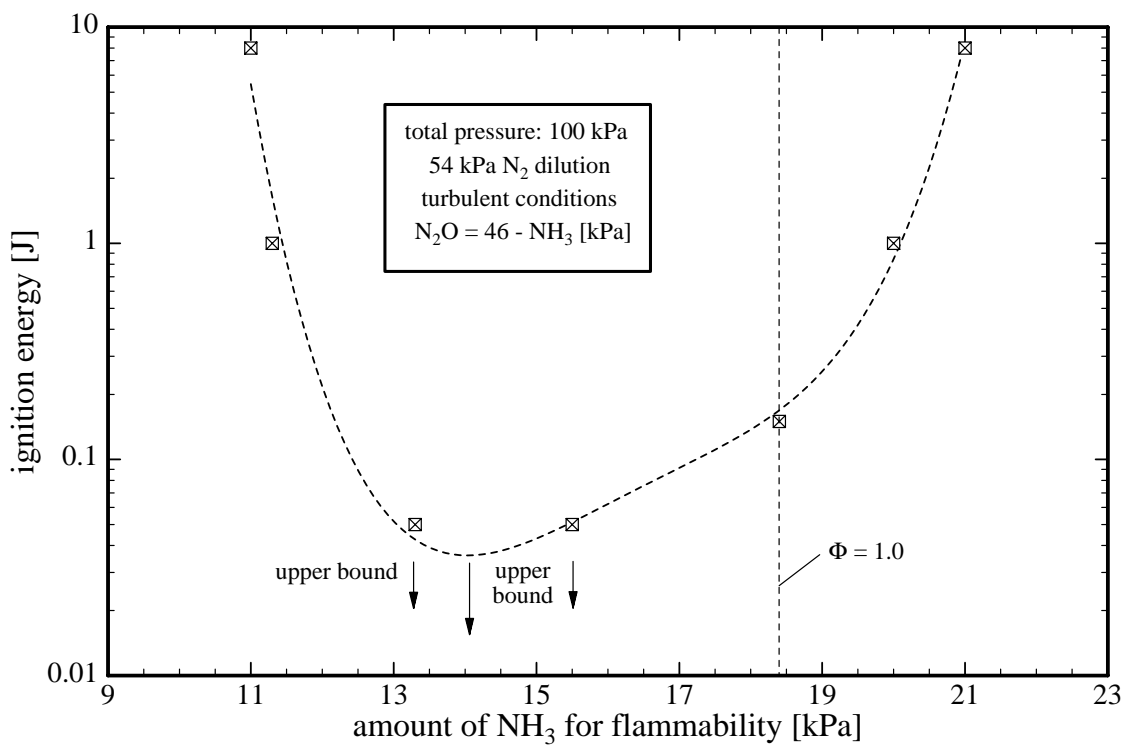
Figure 39: Minimum ignition energy as a function of ammonia concentration at 54 kPa nitrogen dilution.

Run No.	initial NH$_3$ [kPa]	initial N$_2$O [kPa]	ignition energy [J]	final pressure [kPa]	peak pressure bar
456a	4.5	95.5	8.0	-	-
456b	4.75	95.25	8.0	-	-
457	5.0	95.0	8.0	-	-
458	6.0	94.0	8.0	137.6	11.75
464	5.5	94.5	8.0	137.1	11.45
520	6.75	93.25	0.1	-	-
521	7.0	93.0	0.1	-	-
522	7.0	93.0	1.0	134.9	11.4
523	8.0	92.0	0.04	-	-
530	10.0	90.0	0.04	-	-
531	10.0	90.0	0.05	131.7	12.3
532	5.25	94.75	8.0	137.3	11.4
533	5.75	94.25	1.0	137.2	11.4
533a	5.25	94.75	1.0	-	-
533b	5.5	94.5	1.0	-	-
534	7.5	92.5	0.1	135.1	11.9
534a	7.25	92.75	0.1	-	-
535	8.25	91.75	0.05	133.4	11.9
535a	7.5	92.5	0.05	-	-
535b	7.75	92.25	0.05	-	-
535c	8.0	92.0	0.05	-	-
536	13.0	87.0	0.04	127.7	13.0
537	12.0	88.0	0.04	128.4	12.75
538	11.5	88.5	0.04	129.3	12.6
538a	10.75	89.25	0.04	-	-
538b	11.0	89.0	0.04	-	-
538c	11.25	88.75	0.04	-	-

Table 23: Initial gas composition, ignition energy, actual final and peak pressure of NH$_3$–N$_2$O runs (lower limit).

Run No.	initial NH$_3$ [kPa]	initial N$_2$O [kPa]	ignition energy [J]	final pressure [kPa]	peak pressure bar
459a	69.0	31.0	8.0	-	-
460	68.0	32.0	8.0	-	-
461	65.0	35.0	8.0	130.7	11.0
462	67.0	33.0	8.0	131.8	10.1
463	67.5	32.5	8.0	129.8	9.6
539	40.0	60.0	0.04	85.3	15.3
540	59.5	40.5	0.05	121.3	12.6
540a	62.0	38.0	0.05	-	-
540b	61.0	39.0	0.05	-	-
540c	60.0	40.0	0.05	-	-
541	50.0	50.0	0.04	105.1	14.7
541a	58.0	42.0	0.04	-	-
541b	57.0	43.0	0.04	-	-
541c	55.0	45.0	0.04	-	-
542	54.0	46.0	0.04	111.9	14.1
543	58.0	42.0	0.05	118.6	13.1
544	63.0	37.0	0.1	127.0	11.7
544a	65.0	35.0	0.1	-	-
544b	64.0	36.0	0.1	-	-
544c	63.5	36.5	0.1	-	-
545	61.5	38.5	0.1	126.7	12.0
546	66.0	34.0	1.0	129.7	10.5
546a	67.5	32.5	1.0	-	-
546b	66.7	33.3	1.0	-	-

Table 24: Initial gas composition, ignition energy, actual final and peak pressure of NH$_3$–N$_2$O runs (upper limit).

Run No.	initial NH$_3$ [kPa]	initial N$_2$O [kPa]	initial N$_2$ [kPa]	ignition energy [J]	final pressure [kPa]	peak pressure bar
496	10.0	36.0	54.0	8.0	-	-
551	10.5	35.5	54.0	8.0	-	-
552	10.8	35.2	54.0	8.0	-	-
553	10.9	35.1	54.0	8.0	-	-
495	11.0	35.0	54.0	8.0	104.6	8.1
553a	11.0	35.0	54.0	1.0	-	-
554	18.4	27.6	54.0	1.0	94.1	9.37
554a	18.4	27.6	54.0	0.1	-	-
498	22.0	24.0	54.0	8.0	-	-
555	21.5	24.5	54.0	8.0	-	-
556	21.25	24.75	54.0	8.0	-	-
499	21.0	25.0	54.0	8.0	97.6	8.8
557	20.75	25.25	54.0	8.0	96.4	8.8
557a	20.75	25.25	54.0	1.0	-	-
558a	20.0	26.0	54.0	1.0	95.3	9.06
558b	20.0	26.0	54.0	0.1	-	-
559	20.4	25.6	54.0	1.0	-	-
560	19.5	26.5	54.0	1.0	94.6	9.26
560a	19.5	26.5	54.0	0.1	-	-
561a	12.0	34.0	54.0	1.0	102.4	8.35
561b	12.0	34.0	54.0	0.1	-	-
562	11.3	34.7	54.0	1.0	104.2	8.0
562a	11.3	34.7	54.0	0.1	-	-
563a	18.4	27.6	54.0	0.15	94.4	9.3
564	15.5	30.5	54.0	0.05	98.3	8.9
564a	15.5	30.5	54.0	0.04	-	-
565	13.3	32.7	54.0	0.05	101.2	8.6
565a	13.3	32.7	54.0	0.04	-	-

Table 25: Initial gas composition, ignition energy, actual final and peak pressure of NH$_3$–N$_2$O–N$_2$ runs (54% nitrogen dilution, lower and upper limit).

Run No.	initial NH$_3$ [kPa]	initial N$_2$O [kPa]	initial air [kPa]	ignition energy [mJ]	final pressure [kPa]	peak pressure bar
547	21.9	0.0	78.1	100	75.7	7.3
547a	21.9	0.0	78.1	40	-	-
547b	21.9	0.0	78.1	50	-	-

Table 26: Initial gas composition, ignition energy, actual final and peak pressure of NH$_3$–air runs, $\Phi = 1.0$.

8 Mixture 27

Flammability limits, ignition energy bounds and product compositions were determined for mixture 27 (40% H_2, 40% N_2O, 20% CH_4) with air.

8.1 Lean Flammability Limit and Ignition Energy Bounds

At 8 J ignition energy, the lower flammability limit of mixture 27 with air occurs at 7% mixture 27 and there is no upper limit, 100% mixture 27 without air is still flammable. The peak pressures during combustion are shown in Figs. 40 and 41 and compared to STANJAN calculations. Within the range of ignition energy from 0.04 to 8 J, there is almost no measurable shift of the lower flammability limit (see Fig. 42). The initial gas composition, actual final and peak pressure of mixture 27–air runs are given in Table 27 for 8 J ignition energy and in Table 28 for 0.04 J ignition energy.
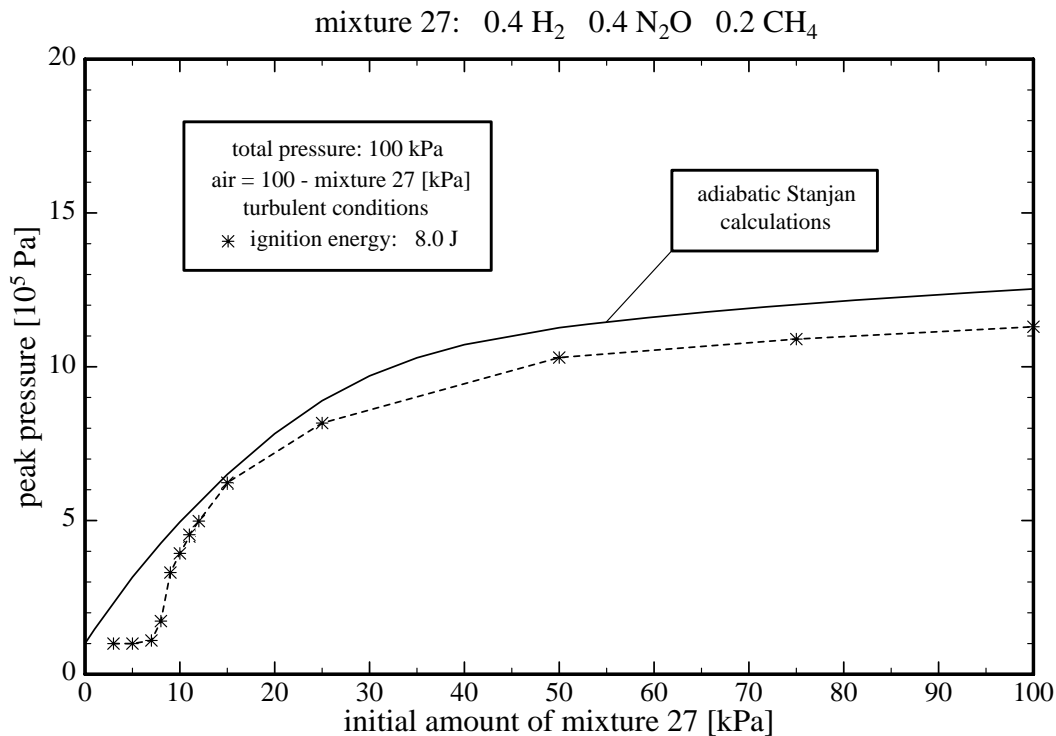

Figure 40: Peak pressure vs. mixture 27 concentration.

Run No.	initial mixture 27 [kPa]	initial air [kPa]	final pressure [kPa]	peak pressure bar
577	11.0	89.0	92.8	4.54
578	100.0	0.0	122.9	11.3
579	50.0	50.0	84.4	10.3
580	75.0	25.0	106.1	10.9
581	25.0	75.0	87.1	8.17
582	3.0	97.0	-	-
582a	5.0	95.0	-	-
583	10.0	90.0	90.2	3.93
584	8.0	92.0	95.4	1.73
585	9.0	91.0	93.2	3.31
586	7.0	93.0	99.1	1.10
590	11.0	89.0	92.5	4.48
591	12.0	88.0	91.8	4.98
592	15.0	85.0	93.5	6.23
593	15.0	85.0	93.6	6.20

Table 27: Initial gas composition, actual final and peak pressure of mixture 27–air runs.

Run No.	initial mixture 27 [kPa]	initial air [kPa]	ignition energy [J]	final pressure [kPa]	peak pressure bar
587	10.0	90.0	0.04	93.0	3.51
588	9.0	91.0	0.04	93.4	3.24
589	8.0	92.0	0.04	105.5	1.59
589a	6.0	94.0	0.04	-	-
589b	7.0	93.0	0.04	-	-

Table 28: Initial gas composition, ignition energy, actual final and peak pressure of mixture 27–air runs.
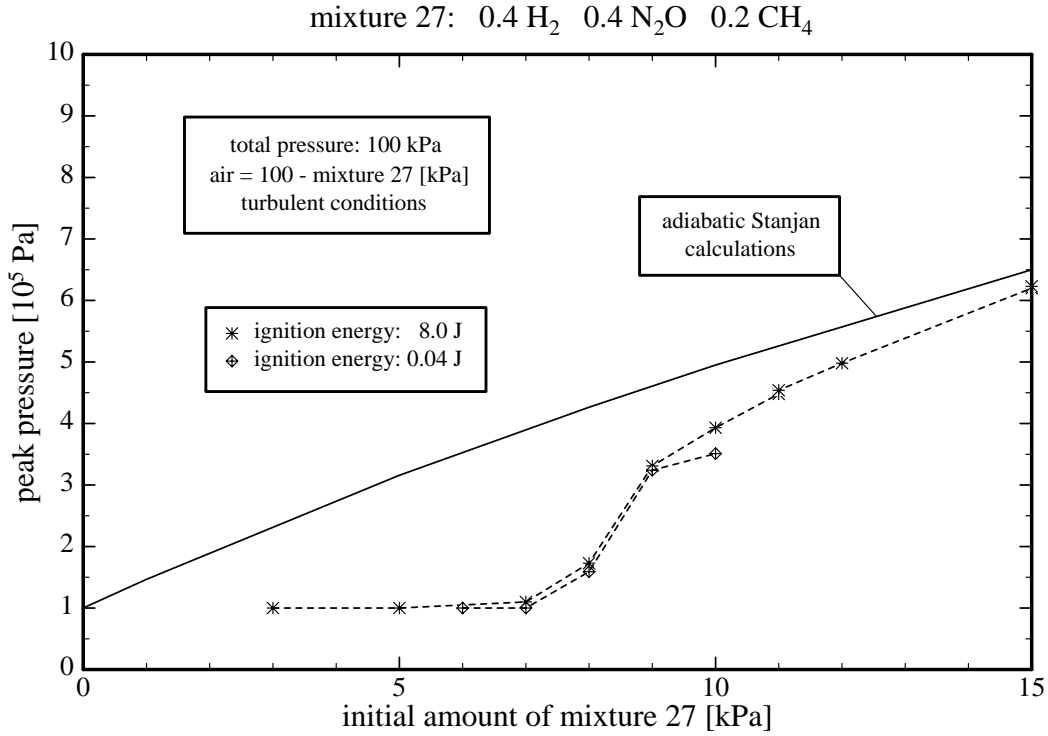
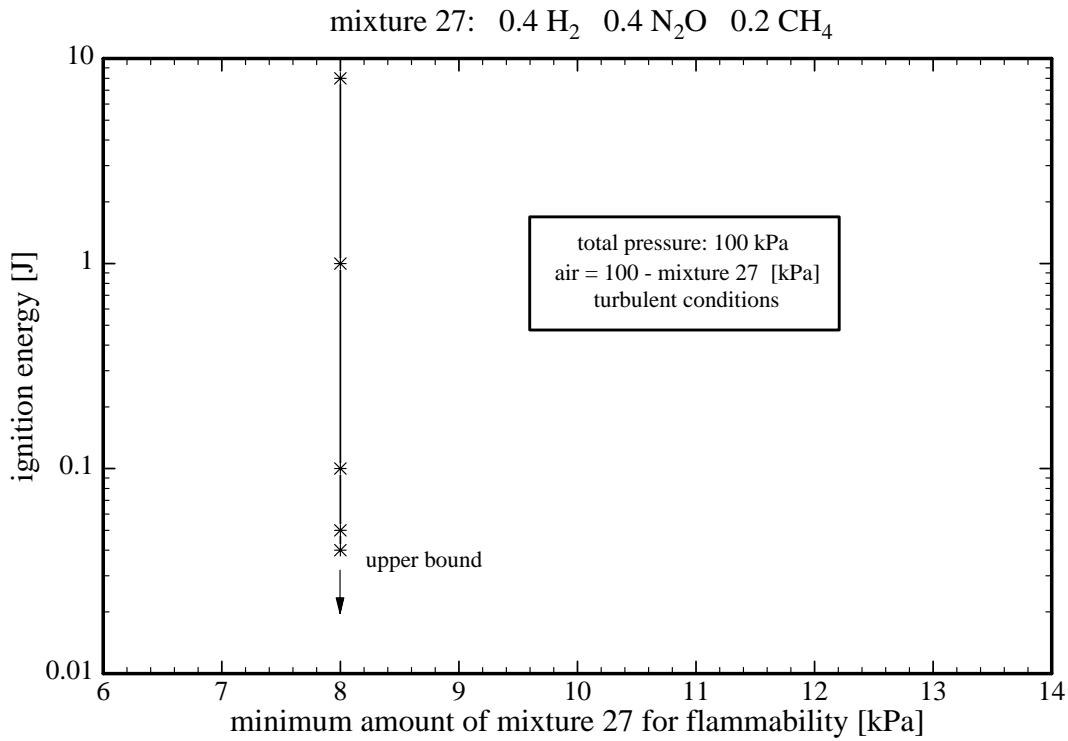Figure 41: Peak pressure vs. mixture 27 concentration for various ignition energies.

Figure 42: Minimum ignition energy as a function of mixture 27 concentration.

Run No.	initial mixture 27 [kPa]	initial air [kPa]	initial H_2 [kPa]	final H_2 [kPa]	initial CH_4 [kPa]	final CH_4 [kPa]	initial N_2O [kPa]	final N_2O [kPa]	final pressure [kPa]	peak pressure bar
589b	7.0	93.0	2.8	2.8	1.4	1.4	2.8	2.8	-	-
589	8.0	92.0	3.2	2.1	1.6	1.2	3.2	3.1	105.5	1.59
588	9.0	91.0	3.6	0.20	1.8	0.15	3.6	2.9	93.4	3.24
587	10.0	90.0	4.0	0.19	2.0	0.11	4.0	2.4	93.0	3.51
590	11.0	89.0	4.4	0.05	2.2	0.03	4.4	0.48	92.5	4.48
591	12.0	88.0	4.8	0.04	2.4	0.02	4.8	0.20	91.8	4.98
592	15.0	85.0	6.0	0.05	3.0	0.02	6.0	0.08	93.5	6.23

Table 29: Initial and final gas composition, actual final and peak pressure of mixture 27–air runs.

8.2 Product Composition

Figure 43 shows the product composition of mixture 27-air combustion near the lean limit. For hydrogen and methane consumption, almost a on/off mechanism can be recognized at the flammability limit. For N_2O consumption, a more gradual transition occurs. The N_2O participation limit occurs at around 10% mixture 27. The initial and final gas composition, actual final and peak pressure of these tests are given in Table 29.
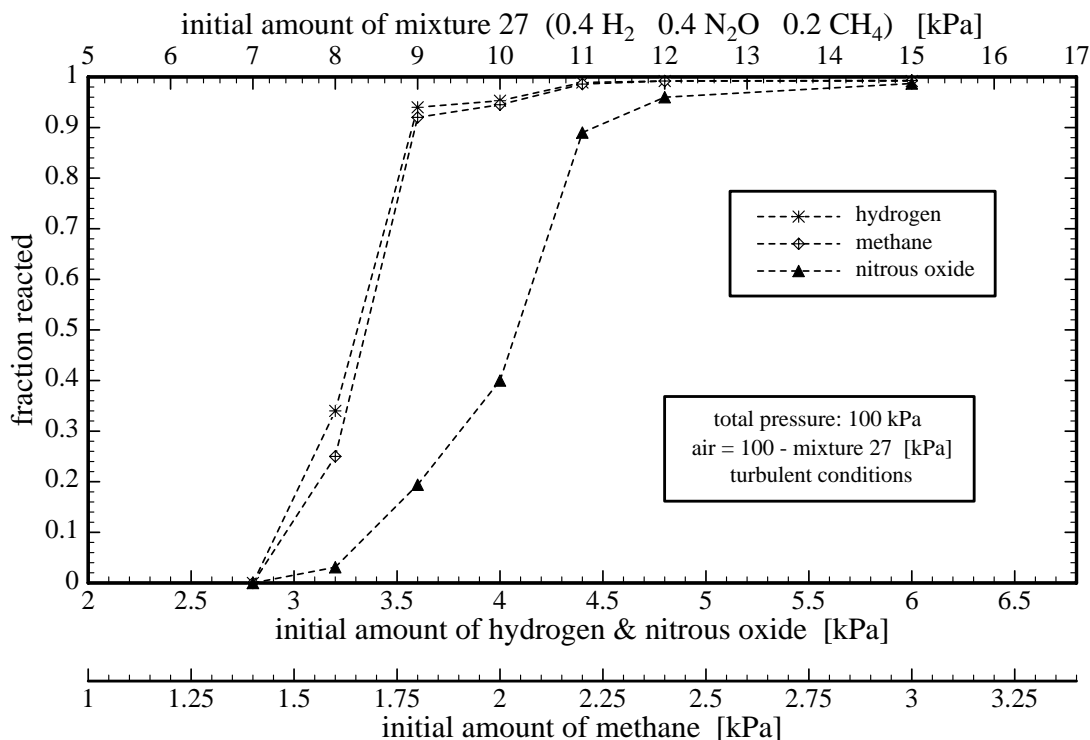

Figure 43: Product composition of mixture 27 - air combustion.

9   Mixture 28

Flammability limits, ignition energy bounds and product compositions were determined for mixture 28 (35% H_2, 35% N_2O, 10% CH_4, 20% NH_3) with air.

9.1   Lean Flammability Limit and Ignition Energy Bounds

At 8 J ignition energy the lower flammability limit of mixture 28 with air occurs at 9% and there is no upper limit, 100% mixture 28 without air are still flammable. The peak pressures during combustion are shown in Figs. 44 and 45 and compared to adiabatic STANJAN calculations. Within the range of ignition energy from 0.04 to 8 J, there is only a very weak shift of the lower flammability limit (see Fig. 46). The initial gas composition, actual final and peak pressure of mixture 28–air runs are given in Table 30 for 8 J ignition energy and in Table 31 for various ignition energies between 0.04 and 1.0 J.
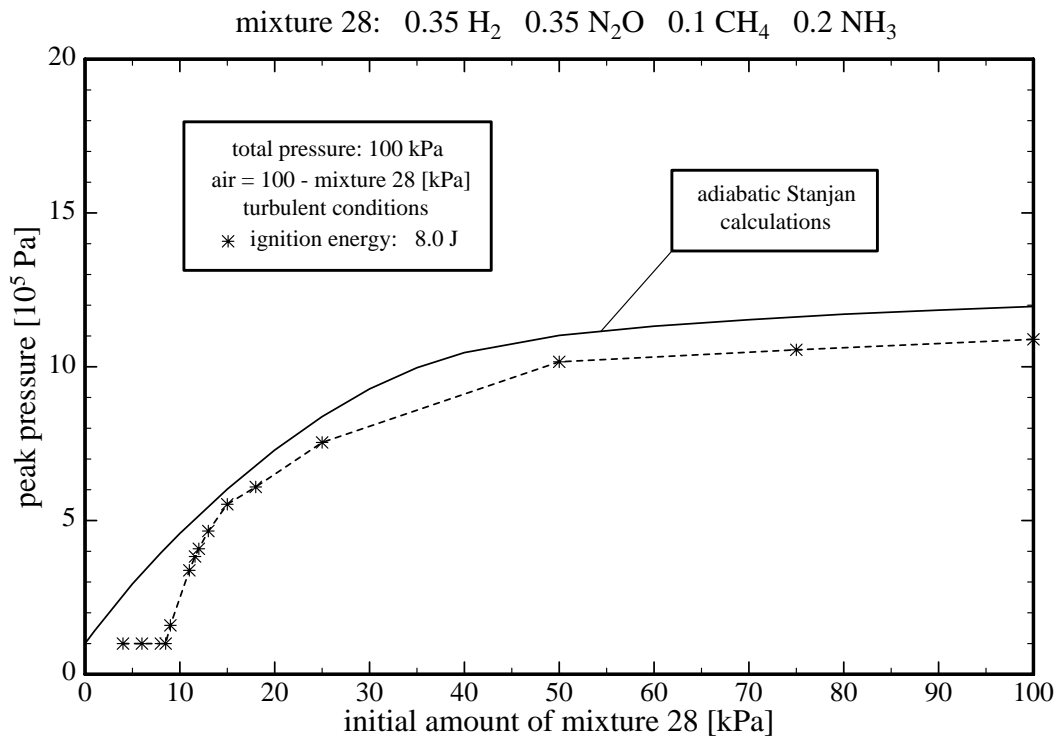

Figure 44: Peak pressure vs. mixture 28 concentration.

Run No.	initial mixture 28 [kPa]	initial air [kPa]	final pressure [kPa]	peak pressure bar
598	11.0	89.0	103.2	3.38
599	15.0	85.0	96.1	5.53
600	13.0	87.0	99.5	4.66
601	12.0	88.0	97.8	4.08
602	18.0	82.0	89.9	6.09
603	11.6	88.4	99.3	3.83
604	9.0	91.0	-	1.59
605	4.0	96.0	-	-
605a	6.0	94.0	-	-
605b	8.0	92.0	-	-
606	100.0	0.0	114.9	10.89
607	75.0	25.0	97.0	10.55
608	50.0	50.0	78.8	10.16
609	25.0	75.0	81.8	7.54
612	8.5	91.5	-	-

Table 30: Initial gas composition, actual final and peak pressure of mixture 28–air runs.

Run No.	initial mixture 28 [kPa]	initial air [kPa]	ignition energy [J]	final pressure [kPa]	peak pressure bar
610	12.0	88.0	0.04	94.5	3.98
611	9.9	90.1	0.05	95.6	2.15
612a	8.75	91.25	1.0	-	-
613	9.0	91.0	1.0	-	-
614	9.2	90.8	1.0	99.0	1.40
615	9.5	90.5	0.05	98.3	1.79
616	10.5	89.5	0.04	94.7	2.71
617	9.3	90.7	0.05	95.4	1.52
618	10.0	90.0	0.04	96.6	2.21

Table 31: Initial gas composition, ignition energy, actual final and peak pressure of mixture 28–air runs.
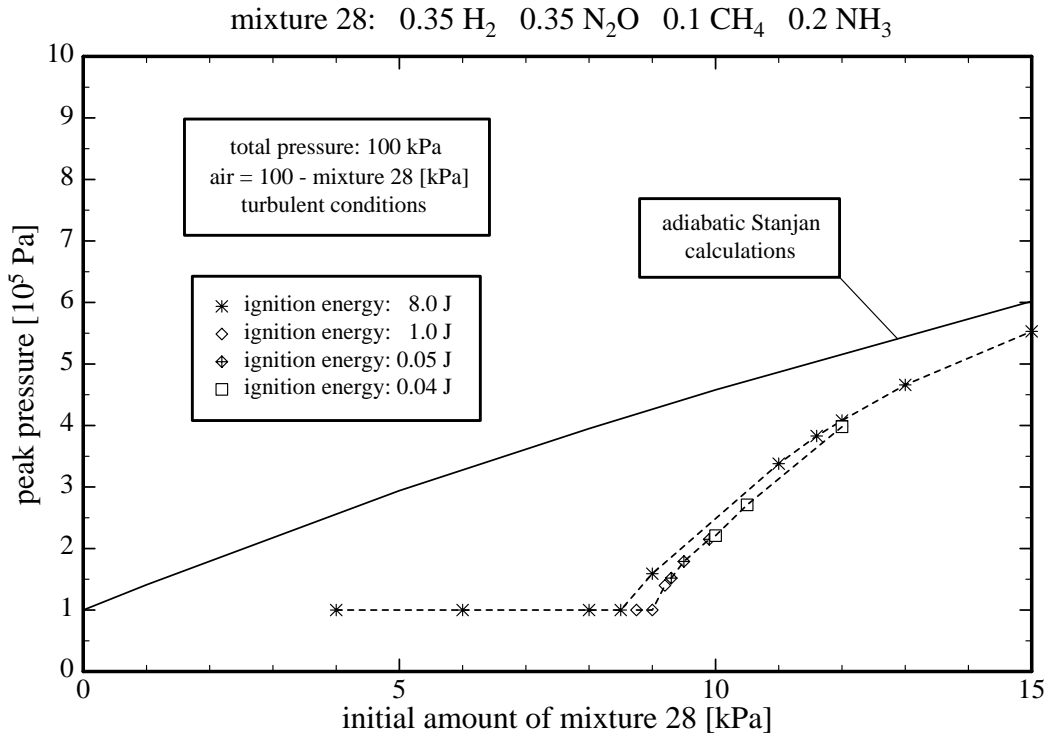
mixture 28:   0.35 H$_2$ 0.35 N$_2$O   0.1 CH$_4$ 0.2 NH$_3$

total pressure: 100 kPa
air = 100 - mixture 28 [kPa]
turbulent conditions

adiabatic Stanjan
calculations

ignition energy: 8.0 J
ignition energy: 1.0 J
ignition energy: 0.05 J
ignition energy: 0.04 J

Figure 45: Peak pressure vs. mixture 28 concentration for various ignition energies.

mixture 28:   0.35 H$_2$ 0.35 N$_2$O   0.1 CH$_4$ 0.2 NH$_3$

total pressure: 100 kPa
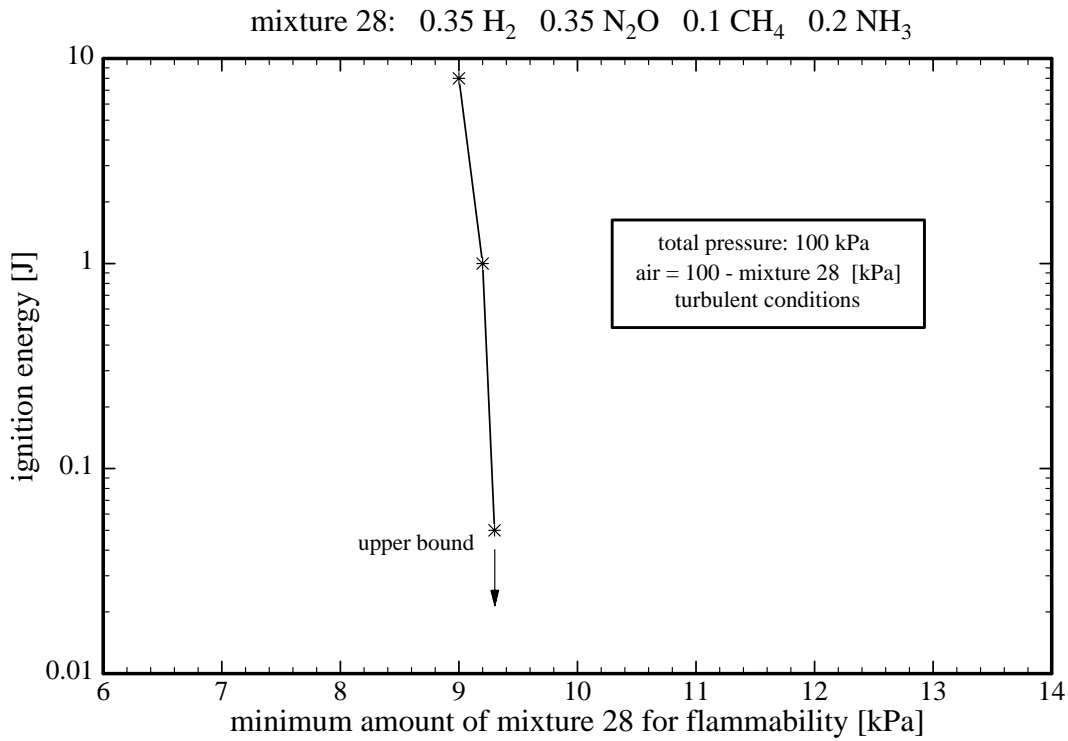air = 100 - mixture 28 [kPa]
turbulent conditions

upper bound

Figure 46: Minimum ignition energy as a function of mixture 28 concentration.

Run No.	initial mixture 28 [kPa]	initial air [kPa]	initial H$_2$ [kPa]	final H$_2$ [kPa]	initial CH$_4$ [kPa]	final CH$_4$ [kPa]	initial N$_2$O [kPa]	final N$_2$O [kPa]	initial NH$_3$ [kPa]	final pressure [kPa]	peak pressure bar
605b	8.0	92.0	2.8	2.8	0.8	0.80	2.8	2.8	1.6	-	-
604	9.0	91.0	3.15	2.3	0.9	0.75	3.15	3.05	1.8	-	1.59
598	11.0	89.0	3.85	0.20	1.1	0.09	3.85	3.7	2.2	103.2	3.38
603	11.6	88.4	4.06	0.10	1.16	0.05	4.06	1.6	2.32	99.3	3.83
601	12.0	88.0	4.2	0.06	1.2	0.03	4.2	1.5	2.4	97.8	4.08
600	13.0	87.0	4.55	0.05	1.3	0.02	4.55	0.54	2.6	99.5	4.66
599	15.0	85.0	5.25	0.05	1.5	0.00	5.25	0.20	3.0	96.1	5.53
602	18.0	82.0	6.3	0.02	1.8	0.00	6.3	0.04	3.6	89.9	6.09

Table 32: Initial and final gas composition, actual final and peak pressure of mixture 28–air runs.

9.2 Product Composition

Figure 47 shows the product composition for combustion of mixture 28-air near the lean limit. The behavior of hydrogen and methane consumption is very similar to the results obtained for mixture 27. The nitrous oxide consumption shows a stronger on/off mechanism with a participation limit of 12% mixture 28. The initial and final gas composition, actual final and peak pressure of the present runs are given in Table 32.
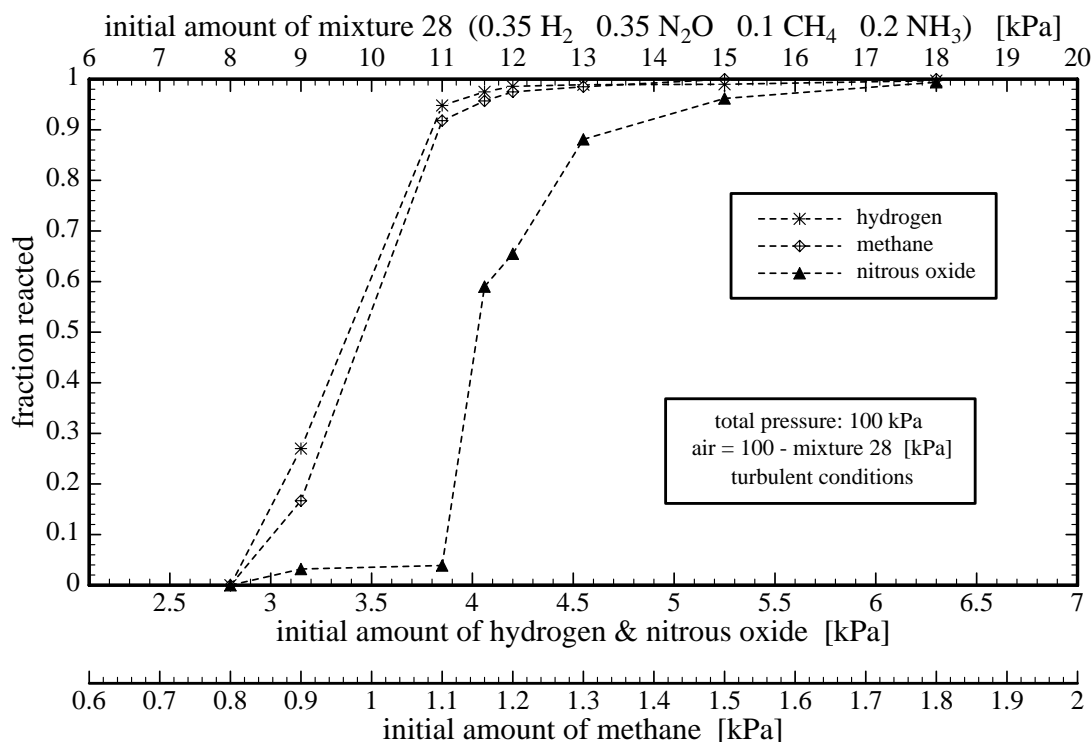

Figure 47: Product composition of mixture 28 - air combustion.

10 Mixture 29

Flammability limits, ignition energy bounds and product compositions were determined for mixture 29 (29% H_2, 24% N_2O, 11% NH_3, 35% N_2, 1% CH_4) with air.

10.1 Lean Flammability Limit and Ignition Energy Bounds

At 8 J ignition energy, the lower flammability limit of mixture 29 with air occurs at 14%, the upper flammability limit occurs between 90 and 100% mixture 29. The peak pressures during combustion are shown in Fig. 48 and compared to adiabatic STANJAN calculations. Within the range of ignition energy from 0.05 to 8 J, we observed no shift of the lower flammability limit (see Fig. 49). The initial gas composition, ignition energy, actual final and peak pressure of mixture 29–air runs are given in Table 33.
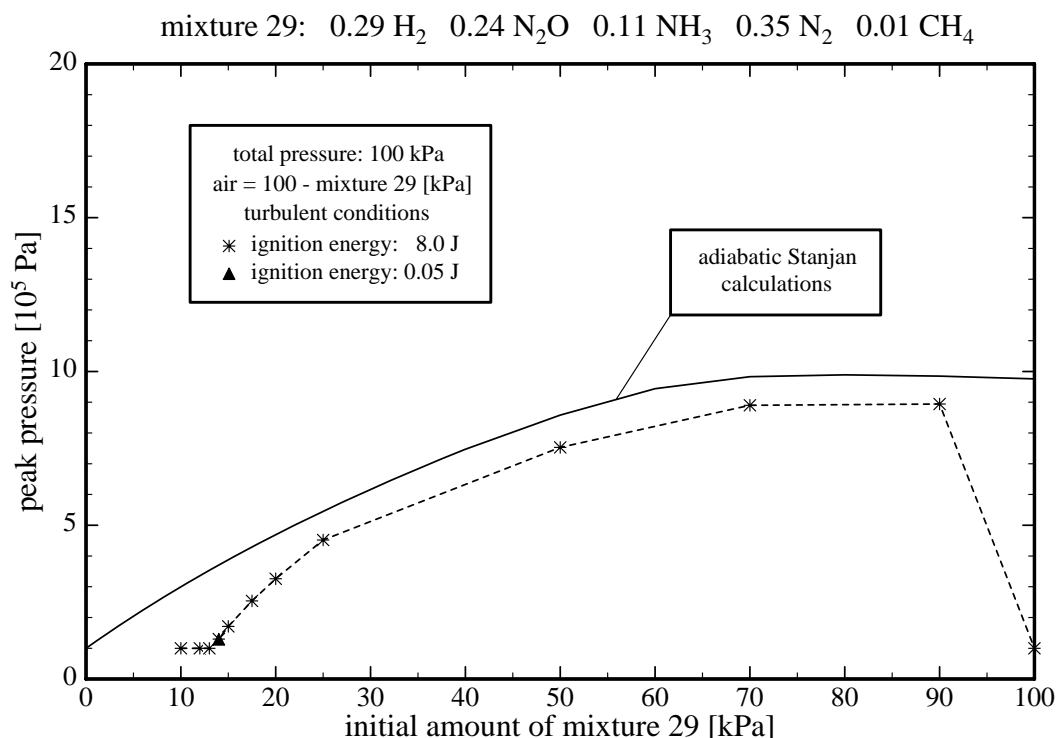

Figure 48: Peak pressure vs. mixture 29 concentration for various ignition energies.

10.2 Product Composition

Figure 50 shows the product composition of mixture 29-air combustion near the lean limit. The behavior of hydrogen consumption is very different from the results obtained for mixture 27 and mixture 28. There is no distinct on/off mechanism around the lower flammability limit. The nitrous oxide consumption shows a smooth increase of N_2O consumption with increasing amount of mixture 29. No sharp nitrous oxide participation limit can be observed. The initial and final gas composition, actual final and peak pressure of the present runs are given in Table 34.

Run No.	initial mixture 29 [kPa]	initial air [kPa]	ignition energy [J]	final pressure [kPa]	peak pressure bar
633	100.0	0.0	8.0	-	-
634	90.0	10.0	8.0	85.7	8.94
635	70.0	30.0	8.0	75.4	8.90
636	50.0	50.0	8.0	79.0	7.53
637	25.0	75.0	8.0	88.9	4.52
638	15.0	85.0	8.0	95.6	1.71
639	10.0	90.0	8.0	-	-
639a	12.0	88.0	8.0	-	-
640	13.0	87.0	0.04	-	-
640a	13.0	87.0	1.0	-	-
640b	13.0	87.0	8.0	-	-
641	14.0	86.0	0.05	101.3	1.29
641a	14.0	86.0	0.04	-	-
642	14.0	86.0	8.0	101.2	1.30
643	20.0	80.0	8.0	90.7	3.26
642	17.5	82.5	8.0	-	2.54

Table 33: Initial gas composition, ignition energy, actual final and peak pressure of mixture 29–air runs.

Run No.	initial mixture 29 [kPa]	initial air [kPa]	initial H_2 [kPa]	final H_2 [kPa]	initial CH_4 [kPa]	initial N_2O [kPa]	final N_2O [kPa]	initial NH_3 [kPa]	final pressure [kPa]	peak pressure bar
640b	13.0	87.0	3.77	3.77	0.13	3.12	3.12	1.43	-	-
641	14.0	86.0	4.06	3.02	0.14	3.36	3.20	1.54	101.3	1.29
638	15.0	85.0	4.35	2.33	0.15	3.6	3.34	1.65	95.6	1.71
643	20.0	80.0	5.8	0.19	0.20	4.8	3.84	2.2	90.7	3.26
637	25.0	75.0	7.25	0.07	0.25	6.0	0.98	2.75	88.9	4.52

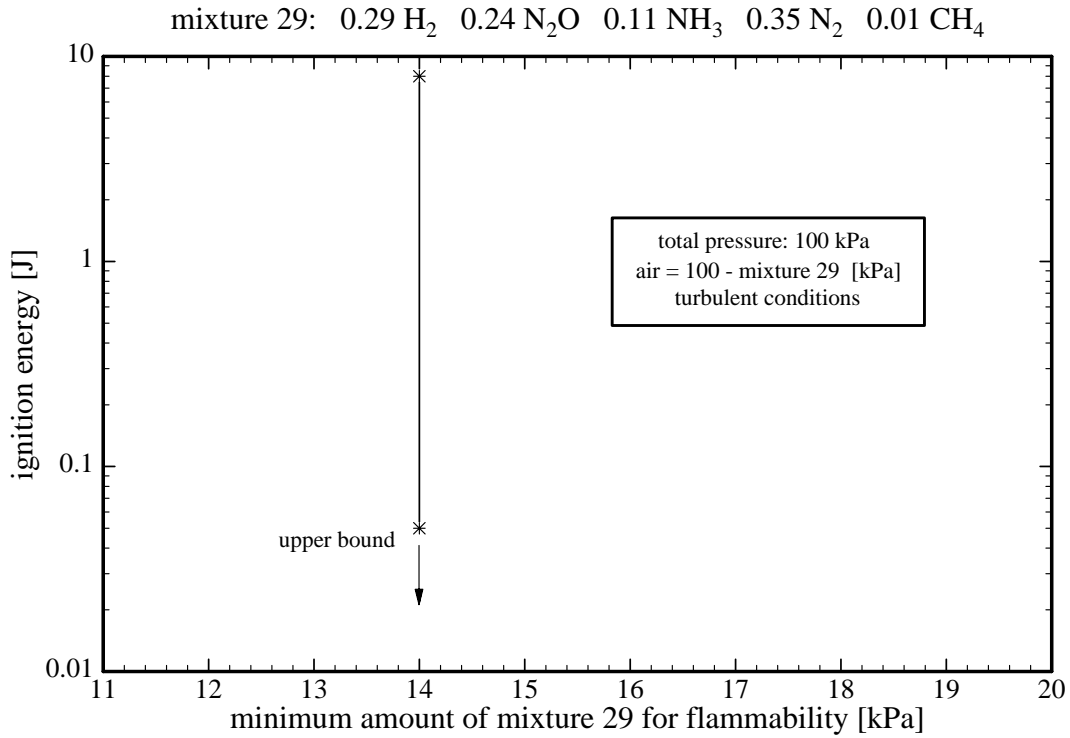Table 34: Initial and final gas composition, actual final and peak pressure of mixture 29–air runs.

mixture 29:   0.29 H$_2$ 0.24 N$_2$O   0.11 NH$_3$ 0.35 N$_2$ 0.01 CH$_4$

Figure 49: Minimum ignition energy as a function of mixture 29 concentration.

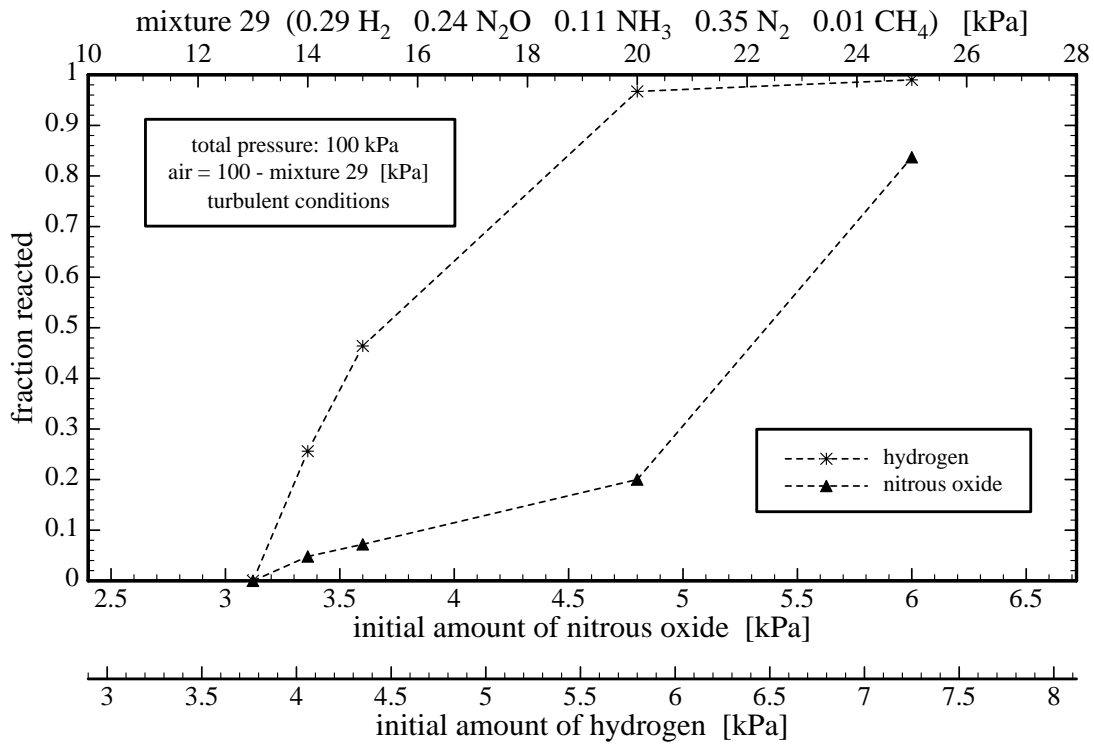mixture 29 (0.29 H$_2$ 0.24 N$_2$O   0.11 NH$_3$ 0.35 N$_2$ 0.01 CH$_4$)   [kPa]

Figure 50: Product composition of mixture 29 - air combustion.

11 Burning Velocities of Mixtures 27 - 29

Burning velocities were measured for mixture 27 (40% H_2, 40% N_2O, 20% CH_4), mixture 28 (35% H_2, 35% N_2O, 10% CH_4, 20% NH_3) and mixture 29 (29% H_2, 24% N_2O, 11% NH_3, 35% N_2, 1% CH_4) in air at quiescent conditions. The initial amounts of mixture 27/28/29 varied between 10 and 20%. The results are shown in Fig. 51. The burning velocities of mixture 27 and mixture 28 in air are very similar, whereas the burning velocities of mixture 29 with air seems to be much slower. The initial gas composition, burning velocity, actual final and peak pressure of the runs are given in Table 35.
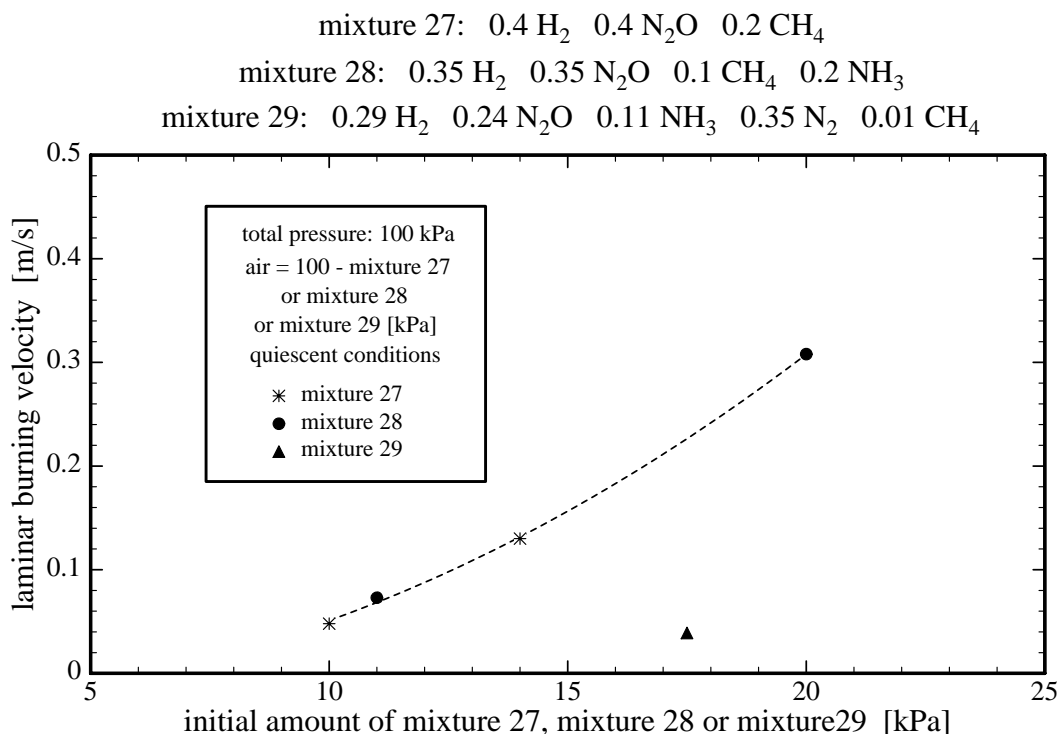

mixture 27: 0.4 H_2 0.4 N_2O 0.2 CH_4

mixture 28: 0.35 H_2 0.35 N_2O 0.1 CH_4 0.2 NH_3

mixture 29: 0.29 H_2 0.24 N_2O 0.11 NH_3 0.35 N_2 0.01 CH_4

Figure 51: Burning velocities of mixtures 27 -29 vs. fuel concentration.

Run No.	initial mixture xx [kPa]	initial air [kPa]	burning velocity [m/s]	final pressure [kPa]	peak pressure bar
	mixture 27				
596	10.0	90.0	0.048	97.9	1.6
594	14.0	86.0	0.13	90.0	5.49
595	75.0	25.0	0.45	102.8	10.84
	mixture 28				
619	11.0	89.0	0.073	99.6	1.70
620	20.0	80.0	0.308	90.3	6.39
	mixture 29				
646	17.5	82.5	0.039	104.3	1.49

Table 35: Initial gas composition, burning velocity, actual final and peak pressure of mixture 27/mixture 28/mixture 29–air runs (quiescent conditions).

For mixture 27, burning velocities were also measured at turbulent conditions. However, these measurements are less meaningful than those at quiescent conditions. The flame surface is quite convoluted and only an average flame speed can be observed. The maximum measurable flame speed is limited by the windows and the time duration between each frame (camera speed). Therefore the results in Fig. 52 for 25 and 50 kPa initial amount of mixture 27 are only lower bounds for the burning velocities. The burning velocity is sligthly higher at 25 than at 50 kPa of mixture 27.
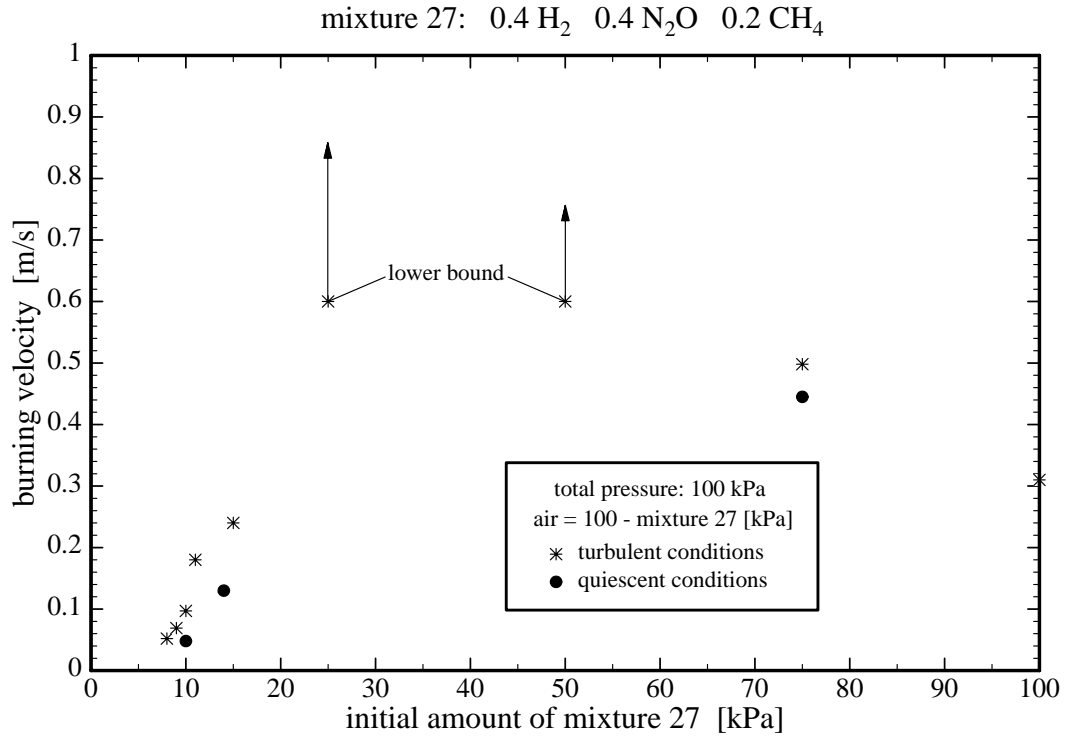
mixture 27: 0.4 H$_2$ 0.4 N$_2$O 0.2 CH$_4$

Figure 52: Mixture 27: comparison between laminar (quiescent conditions) and turbulent burning velocity.

12   Conclusions

This study complements the previous work and rounds out our knowledge of combustion in mixtures containing components found in the flammable gases retained within the waste at the Hanford tank farm. This study has provided significant new data on the following combustion problems

1. The fraction of N_2O reacted in lean hydrogen–nitrous oxide–air, methane–nitrous oxide–air and ammonia–nitrous oxide–nitrogen mixtures and selected waste gas simulants (H_2-N_2O-N_2-NH_3-CH_4 blends, mixtures a - d) mixed with air has been quantified.

2. The behavior of methane–nitrous oxide–nitrogen mixtures has been studied in detail.

3. Flammability limits and inerting concentrations of ammonia–nitrous oxide–nitrogen and ammonia–nitrous oxide–air mixtures have been quantified.

4. Ignition energy bounds of ammonia–nitrous oxide mixtures (rich and lean, with and without nitrogen dilution) have been measured.

5. Flammability limits, ignition energy bounds, flame speeds and product compositions of selected hydrogen–nitrous oxide–ammonia–methane–nitrogen mixtures (mixtures 27 - 29) have been investigated.

The current study required both expanding our capabilities (gas sampling and measurement) and restricting operations in other areas (smaller vessel, operation without windows).

The present investigations were carried out in the 11-liter vessel since high pressures (up to 12 bar) are consistently produced with mixtures containing substantial amounts of N_2O. The 11-liter vessel reduces the total amount of gas by a factor of 40 over the CONVOL vessel that was used in previous tests. This is important both from the viewpoint of minimizing the total energy of explosives in the lab and in reducing the heat load on the vessel. Preliminary testing with CONVOL indicated that a cooling system would have to be installed in order to use mixtures with substantial amounts of N_2O if more than one test per day were performed.

High-speed flames and the potential for DDT are an issue in the laboratory experiments that form an important constraint on operations with substantial amounts of N_2O. For many of the present tests, measurements were made without the schlieren system since the windows were damaged in preliminary tests with high N_2O fraction mixtures. Operation with windows also poses a safety hazard in this regime.

This means that flame speed measurements could not be made on many of these experiments. In addition, the current technique for flame speed measurement relies on the video recording system to acquire images for later processing. In systems containing large amounts of N_2O, the flames are sufficiently fast that the video system is inappropriate. Future studies should consider alternate flame speed measurement techniques.

References

Andrews, D. G. R. and P. Gray (1964). Combustion of ammonia supported by oxygen, nitrous oxide or nitric oxide: laminar flame propagation at low pressures in binary mixtures. *Combustion and Flame 8*, 113–126.

Armitage, J. W. and P. Gray (1965). Flame speeds and flammability limits in the combustion of ammonia: ternary mixtures with hydrogen, nitric oxide, nitrous oxide or oxygen. *Combustion and Flame 9*, 173–184.

Breshears, W. D. (1995). Falloff behavior in the thermal dissociation rate of N_2O. *Journal of Physical Chemistry 99*, 12529 – 12535.

Buckley, W. L. and H. W. Husa (1962). Combustion properties of ammonia. *Chemical Engineering Progress 58, 2*, 81–84.

Calcote, H. F., J. C. A. Gregory, C. M. Barnett, and R. B. Gilmer (1952). Spark ignition. *Industrial and Engineering Chemistry 44, 11*, 2656–2662.

Cashdollar, K., M. Hertzberg, I. Zlochower, C. Lucci, G. M. Green, and R. A. Thomas (1992, June). Laboratory flammability studies of mixtures of hydrogen, nitrous oxide, and air. Final Report WHC-SD-WM-ES-219, Bureau of Mines.

Coward, H. F. and G. W. Jones (1952). Limits of flammability of gases and vapors. Bulletin 503, Bureau of Mines.

Fenton, D. L., A. S. Khan, R. D. Kelley, and K. S. Chapman (1995). Combustion characteristics review of ammonia–air mixtures. *ASHRAE Transactions 3922*, 1–10.

Hertzberg, M. and I. Zlochower (1993). Explosibility of nitrous oxide gas: The effect of H-atom-bearing impurities. Abstract, Joint Meeting of British and German Sections of the Combustion Institute, March 29-April 3, Cambridge, England.

Jones, E. and J. Kerr (1949). Inflammability limits of ammonia, nitrous oxide, and air. *J.S.C.I. 68*, 31–34.

Jorissen, W. P. and B. L. Ongkiehong (1926). The explosion regions of hydrogen–ammonia–air and hydrogen–ammonia–oxygen mixtures. *Rec. trav. chim. 45*, 224–231.

Kuchta, J. (1985). Investigation of fire and explosion accidents in the chemical, mining, and fuel-related industries—a manual. Bulletin 680, U.S. Bureau of Mines.

Posthumus, K. (1930). On explosion regions of gas mixtures, in which one or two of the gases are endothermic. *Rec. trav. chim. 49*, 309–347.

Reynolds, W. C. (1986, January). *The Element Potential Method for Chemical Equilibrium Analysis: Implementation in the Interactive Program STANJAN* (3rd ed.). Dept. of Mechanical Engineering, Stanford, CA: Stanford University.

Ronney, P. D. (1985). Effect of gravity on laminar premixed gas combustion ii: ignition and extinction phenomena. *Combustion and Flame 62*, 121–133.

Ross, M. C. and J. E. Shepherd (1996, July). Lean combustion characteristics of hydrogen-nitrous oxide-ammonia mixtures in air. part i. Explosion Dynamics Lab Report FM96-4, California Institute of Technology, Pasadena, CA.

Scott, F. E., R. W. V. Dolah, and M. G. Zabetakis (1957). The flammability characteristics of the system H_2–no–N_2O–air. In *Sixth Symp. (Intl) Combustion*, Pittsburgh, PA, pp. 540–545. The Combustion Institute.

Shebeko, Y. N., S. G. Tsarichenko, A. Y. Korolchenko, A. V. Trunev, V. Y. Navzenya, S. N. Papkov, and A. A. Zaitzev (1995). Burning velocities and flammability limits of gaseous mixtures at elevated temperatures and pressures. *Combustion and Flame 102*, 427–437.

Smith, S. and J. W. Linnett (1953). The upper limits of inflammability of hydrogen–air and hydrogen–nitrous oxide mixtures. *J. Chem. Soc. (London) Part I*, 37–43.

van der Wal, M. J. (1934). Explosive and nonexplosive reactions between nitrogen oxides and flammable gases. *Rec. trav. chim. 53*, 97–117.

White, A. G. (1922). Limits for the propagation of flame at various temperatures in mixtures of ammonia with air and oxygen. *J. Chem. Soc. 121*, 1688–1695.

Zabetakis, M. G. (1965). Flammability characteristics of combustible gases and vapors. Bulletin 627, Bureau of Mines.